Anomalous Aspects of Magnetosheath Flow and of the Shape and Oscillations of the Magnetopause During an Interval of Strongly Northward Interplanetary Magnetic Field

SHENG-HSIEN CHEN,[1,2] MARGARET G. KIVELSON,[1,2] JACK T. GOSLING,[3] RAYMOND J. WALKER,[1] AND ALLAN J. LAZARUS[4]

On February 15, 1978, the orientation of the interplanetary magnetic field (IMF) remained steadily northward for more than 12 hours. The ISEE 1 and 2 spacecraft were located near apogee on the dawnside flank of the magnetotail. IMP 8 was almost symmetrically located in the magnetosheath on the dusk flank and IMP 7 was upstream in the solar wind. Using plasma and magnetic field data, we show that (1) the magnetosheath flow speed on the flanks of the magnetotail steadily exceeded the solar wind speed by 20%, (2) surface waves of ~5-min period and very nonsinusoidal waveform were persistently present on the dawn magnetopause and waves of similar period were present in the dusk magnetosheath, and (3) the magnetotail ceased to flare at an antisunward distance of 15 R_E. We propose that the acceleration of the magnetosheath flow is achieved by magnetic tension in the draped field configuration for northward IMF and that the reduction of tail flaring is consistent with a decreased amount of open nagnetic flux and a larger standoff distance of the subsolar magnetopause. Results of a three-dimensional magnetohydrodynamic simulation support this phenomenological model.

INTRODUCTION

The magnetosheath separates the bow shock from the magnetopause. The solar wind plasma, which is superfast magnetosonic, slows to a speed below the local fast magnetosonic speed across the bow shock. The slowed flow in the magnetosheath is diverted around the magnetopause, continues along the flanks, and then speeds up to the solar wind velocity in the downstream magnetotail. Considerable attention has been directed to the consequences of the coupling of the magnetosheath to the magnetosphere. In particular, it is well known that the magnetosheath flow drives plasma convection in the magnetosphere both through a viscous interaction between the magnetosheath and magnetospheric plasmas at the magnetopause boundary layers [*Axford and Hines,* 1961; *Axford*, 1964] and through magnetic reconnection between the magnetosheath magnetic field and the magnetic field of the magnetosphere [*Dungey*, 1961]. However, less attention has been directed at fully characterizing the magnetosheath itself (but see *Saunders* [1990], *Song et al.* [1990*b*], and *Southwood and Kivelson* [1992]) or at examining details of the coupling between the magnetosheath and the magnetosphere along the flanks of the tail (but see *Gosling et al.* [1986], and *Saunders* [1990]). In this paper, we use data from an interval of persistent northward interplanetary magnetic field (IMF) to study aspects of magnetosheath flow and the nature of its coupling to the magnetopause on the flanks of the magnetotail.

Our analysis focuses on ISEE 1 and 2 data for a 4-hour interval on February 15, 1978, that reveals anomalous ultralow frequency (ULF) perturbations at the tail magnetopause and the low-latitude boundary layer (LLBL). We use plasma data from the Fast Plasma Experiment (FPE) of ISEE 2 and the crossed fan analyzer (X Fan) of ISEE 1 [*Bame et al.*, 1978]. Supporting data are obtained from the MIT faraday cup and Los Alamos National Laboratory electrostatic analyzer [*Bame et al.*, 1967] on IMP 7 and IMP 8. Data from the ISEE 1 and 2 magnetometers [*Russell*, 1978] and the IMP 8 magnetometer (R. P. Lepping et al., IMP 8 solar wind magnetic field and plasma data in support of the Ulysses-Jupiter encounter: 13–31 January 1992, unpublished manuscript, 1992) are also used. The ISEE 1 and 2 spacecraft were near their apogees at ~0300 local time. IMP 7 was in the upstream solar wind. IMP 8 was in the magnetosheath on the duskside. Lacking a magnetometer in the upstream solar

wind, we use magnetic field measurements in the magnetosheath to infer that the orientation of the IMF was strongly northward.

A detailed description of the observations is given in the next section. We show that the flow velocity on the magnetosheath side of the magnetopause exceeded the solar wind speed. This observation can be linked to earlier observations of the magnetosheath on the flanks reported by *Howe and Binsack* [1972]. They showed that the flow velocity in the tail magnetosheath (-20 $\gtrsim X_{GSM} \gtrsim$ -60 R_E) correlated weakly with distance from the magnetopause. Some of the flow velocities at distances $X_{GSM} \gtrsim$ -40 R_E in the magnetosheath were $\sim$10% higher than in the upstream solar wind, but the study did not investigate the effects of IMF orientation.

Flows at speeds greater than the solar wind speed are not found in gasdynamic models of the magnetosheath. For example, the gasdynamic model of *Spreiter et al.* [1966] shows that the magnetosheath flow accelerates gradually downstream of the subsolar point and its speed varies with distance from the magnetopause but the flow velocity never becomes greater than that of the upstream solar wind. *Gosling et al.* [1986] showed evidence of accelerated plasma flows at the near-tail magnetopause ($0 > X_{GSM} > -12.5\ R_E$). They found that the accelerated flows were likely to occur when the terrestrial and magnetosheath magnetic fields were antiparallel and to be found on the magnetospheric side of the magnetopause. They attributed the acceleration to antiparallel merging. However, in our case the accelerated flows were observed in the near-tail magnetosheath and occurred for nearly parallel magnetotail and magnetosheath fields.

In interpreting the data, we attribute anomalous acceleration to the effect of magnetic tension exerted by the IMF on the plasma in the magnetosheath. Our interpretation gives insight into characteristics of magnetosheath flow and its role in exciting surface waves on the magnetopause. A model of accelerated flows in the magnetosheath and an MHD simulation of the model follow. Finally, we discuss implications of our results.

OBSERVATION

In this study we have used multispacecraft observations to investigate a 4-hour interval (1400–1800 UT) when ISEE 2 moved repeatedly from the magnetosheath to the magnetosphere. We start with an overview of the observations earlier on February 15, 1978. These observations show that ISEE 2 was near the magnetopause for most of the day.

The positions of the spacecraft used in our analysis relative to a nominal magnetosphere are shown in Figure 1. Empirical bow shock [*Howe and Binsack*, 1972; *Farris et al.*, 1991] and magnetopause [*Howe and Binsack*, 1972; *Petrinec et al.*, 1991; *Sibeck et al.*, 1991] (as labeled) models are indicated (the solid curves). The dotted curve shows a possible position of the magnetopause in our event. It is obtained by fitting a curve through two points (the position of a model subsolar, dawn-dusk magnetopause of *Sibeck et al.* [1991] for an IMF $B_Z \simeq$ 10 nT and the position of ISEE 2 during boundary layer crossings) and assuming that the magnetopause is symmetric about an aberrated X_{GSM}. The Earth's dipole tilt at the time of our event is small and therefore the hinging of the magnetotail is negligible. The position of the neutral sheet then is close to Z_{GSM}= 0. As the distance between ISEE 1 and ISEE 2 was only a few hundred kilometers, the magnetic field at ISEE 1 during magnetopause crossings differed from that at the ISEE 2 only by a time delay of $\sim$0.65 s. Therefore, we use only the ISEE 2 magnetometer for the analysis.

Figure 2 shows the upstream solar wind conditions observed by IMP 7. Both the Los Alamos National Laboratory (LANL) plasma instrument (Figure 2*a*) and the Massachusetts Institute of Technology (MIT) plasma instrument (Figure 2*b*) on IMP 7 found that the upstream solar wind speed was between 540 and 580 km/s, the ion temperature was a few electron volts and the density was $\sim$3 cm^{-3} during the interval 1400–1800 UT. Note that the MIT plasma data on IMP 7 was contaminated with noise from the spacecraft systems. A few of the spectra on this day indicated densities an order of magnitude greater than those shown here. The high densities were all due to especially large currents in one or rarely two energy channels, all at the same viewing angle. Similar spectra appeared on the following day. There are no magnetic field observations to correlate with, and elimination of the high density spectra bring the MIT parameters into agreement with those made by the LANL instrument. Our conclusion is that those spectra are most probably spurious, and they have been eliminated from the figure.

Figure 3 shows a 24-hour overview plot of the data from ISEE 2. ISEE 2 passed its apogee at $\sim$1240 UT, shortly before repeatedly encountering the magnetopause between 1400 and 1800 UT. During the interval 1400–1800 UT, the distance of ISEE 2 above the neutral sheet changed from $\sim$6 to 2 R_E. The maximum distance above the neutral sheet during the day was $\sim$8 R_E at $\sim$0900 UT. Using the plasma properties and the magnetic field strength observed by ISEE 2 as guides, we divide the data from the day into seven different portions. In the first region (labeled 1 in Figure 3), the ion bulk flow velocity was low on average, the ion temperature was $\sim$2–4 keV, which is a typical plasma sheet ion temperature, and the ion number density was $\sim$2–3 cm^{-3}. We suggest that this was a plasma sheet encounter including pulses of boundary layer plasma at 0010, 0120 and 0220 UT and possible magnetopause crossings near 0308 and 0405 UT.

Following the plasma sheet encounter (after 0500 UT) a region of fast tailward ion bulk flow ($V_X \simeq$-550 km/s) was encountered. The ion temperature dropped to hundreds of electron volts and the density dramatically increased to 30 cm^{-3}. The IMP 8 data (Figure 4) for this interval showed a high ion number density in the magnetosheath (40–80 cm^{-3}) accompanied by an ion bulk flow velocity of $\sim$600 km/s and a strong magnetic field ($\sim$40 nT, see Figure 5). Thus, the region labeled 2 in Figure 3 represents ISEE 2's entry into the solar wind plasma in the magnetosheath. There are also magnetopause crossings at $\sim$0835 and 0840 UT. The flow velocity moment provided by the FPE instrument on ISEE 2 is calculated assuming that the ions uniformly fill the $\pm$55° acceptance fan of the analyzer. Whereas this assumption is generally valid in the magnetosphere, it is not appropriate in the magnetosheath. The true magnetosheath velocity is higher than the FPE moment. No such assumption is made for moments calculated from measurements of the X fan instrument on ISEE 1. Below we show that the X fan instrument obtains higher speeds than does the FPE in the magnetosheath, and that the magnetosheath speed in the dawn flank is approximately equal to that measured on the dusk flank by IMP 8.

After passing through the plasma sheet at 0850–0910 UT, the bulk flow velocity in Figure 3 decreased again and the number density dropped to a value less than 1 cm^{-3}. The temperature changed little other than during a brief interval close to the temporal change, and the magnetic field strength went up to $\sim$70 nT. If we recall that ISEE 2 reached its largest distance from the model neutral sheet at $\sim$0900 UT we may conclude that the spacecraft entered the lobe or the plasma mantle (labeled 3 in Figure 3). Examination of distribution functions provides the following detail for the spacecraft location: the plasma mantle at 0910–0940 UT, the lobe at

0940–1005 UT, and again the plasma mantle at 1005–1020 UT.

After ~1020 UT, ISEE 2 returned to the magnetosheath where it remained for approximately an hour (labeled 4 in Figure 3). Starting at ~1130 UT, ISEE 2 was in the plasma sheet until ~1400 UT (labeled 5 in Figure 3). After that a strong tailward flow was observed again (labeled 6 in Figure 3) and the flows persisted for 4 hours. This is the interval of particular interest in this paper. During the interval, all of the plasma parameters fluctuated greatly, and below we will provide evidence that the spacecraft passed back and forth between the magnetosheath and the low-latitude boundary layer.

From the IMP 8 observations after 1400 UT (Figures 4 and 5), we recognize that the plasma conditions in the duskside magnetosheath changed to a relatively steady state (n_i= 4 cm^{-3}, V_i= 700 km/s, and a strongly northward IMF) and these conditions persisted for 4 hours. Figure 5 shows that during the first half of the day, the field observed at IMP 8 was quite variable. During the long interval of southward field from 0900 to 1140 UT, the field at ISEE 2 which was in the lobe became more taillike and grew in amplitude. Shortly after, ISEE 2 entered the magnetosheath. After 1400 UT, large values for B_z and small B_x and B_y components were seen at both the ISEE 2 and the IMP 8 spacecraft on opposite flanks of the magnetopause. The average values in nanoteslas of the magnetic field components in the magnetosheath were (5, 5, 40) and (8, -4, 28) at the dawnside and the duskside, respectively. Our inference that the IMF orientation was principally northward with a small sunward inclination follows from these measurements. A northward pointing field is dragged over the flanks by the flow and drapes around the magnetopause. At positions near the equator in the northern hemisphere, that is, at the positions of ISEE 2 at dawn and IMP 8 at dusk, small and oppositely directed y components arise from the draping. The positive x component suggests that the upstream field was inclined sunward.

As mentioned above, in the interval 1400–1800 UT, the magnetic field components, ion bulk velocity, density, pressure and temperature fluctuated significantly at ISEE 2. This is the interval of interest to us; we will examine it in detail below. After 1800 UT the amplitude of the fluctuations of plasma and magnetic field properties decreased at ISEE 2 (Figure 3, interval 7) and their average values gradually departed from magnetosheath character. Finally after ~2100 UT, ISEE 2 returned to the plasma sheet for the remainder of the day.

In the remainder of the paper, we focus on specific aspects of the data. Analysis of the fluctuations will lead to the conclusion that surface waves on the boundary produced the plasma and field signatures observed at ISEE 2 between 1400 and 1800 UT. The unexpected acceleration of the solar wind from its upstream values of between 540 and 580 km/s during the 4-hour event (Figures 2*a* and 2*b*) to a larger downstream value at both ISEE 1 and IMP 8 will be further examined and interpreted.

BOUNDARY FLUCTUATIONS

To study in detail the abnormal fluctuations present during the entire time interval from 1400 to 1800 UT, we examine 4-s field and 12-s plasma (3-s snapshot) data from a representative 1-hour interval. Figure 6 shows data for the interval from 1500 to 1600 UT. The vertical dashed lines separate similar structures based on the differences of plasma properties and magnetic field components. The vertical dashed lines are placed at times just before the ion density starts to increase significantly. The variations of the ion number density, the ion bulk flow velocity

and the magnetic field strength were inphase to zeroth order. The ion temperature, however, was out of phase with these signatures. The B_x component changed to a negative value as the ion density increased, and became positive before the density went down. There are ~20-nT and ~30- to 40-nT peak-to-peak variations in the dominant component B_z and in the transverse component B_x, respectively. Repeated traversals of the magnetopause, which is approximately normal to $\hat{y}$, would be consistent with this signature.

In order to interpret the quasi-periodic variations observed, we provide further details for a single cycle at 1540–1550 UT. Figure 7 gives the plasma parameters, the magnetic field components and six selected snapshots of electron and ion distribution functions which represent different plasma regimes. The 4-s average values of the magnetic field projection onto the X-Y_{SC} plane are drawn on top of the electron contours. The first and last pairs of distribution functions show the properties of the LLBL with cold electrons streaming along the field lines and hot electrons perpendicular to the field lines [*Ogilvie et al.*, 1984; *Takahashi et al.*, 1991]. Note that the angles between the X-Y_{SC} plane and the magnetic field at 1544 UT (the first panel of Figure 7*b*) and 1549 UT (the last panel) are ~27° and ~43°, respectively. The field of view of the plasma instrument was ±55° and, therefore, the components of field-aligned streaming electrons on the X-Y_{SC} plane can be seen. It is well known that the plasma in the magnetosheath is colder and denser than in the LLBL. The fourth pair of distribution functions in Figure 7*b* are typical for magnetosheath plasma. Both ions and electrons are cold and there is no field-aligned electron streaming. The rest of the distribution functions have properties intermediate between the magnetosheath and the LLBL. The electron contours reveal a time-aliasing effect (the starlike shape of contours) in the second and fifth pairs in Figure 7*b*. The time-aliasing effect was caused by a rapid displacement of a boundary across ISEE 2 within the 3-s of an FPE snapshot. The FPE instrument contains two detectors looking in opposite directions and is operating in an interleaved-angle mode in which two measurements at adjacent angles are made during different halves of a spin cycle and are, therefore, separated by 1.5 s. The third pair of distribution functions shows characteristics much like those of the LLBL. However, the magnetic field direction in the third pair is different from that of the LLBL (the first and last pairs in Figure 7*b*). Following the classifications of *Song et al.* [1990*a*], the third pair of distribution functions may be an outer LLBL with the first and last pairs corresponding to inner LLBLs and the second and fifth pairs being sheath transition layers. Since the classification of the LLBL is not unique, we keep the question open. Based on the very rapid perturbations of magnetic field (Figure 7 or Figure 6), strong current layers were present at the magnetopause, especially during entries into the magnetosheath.

Our analysis has relied on plasma data from the FPE instrument on ISEE 2. However, the calculated moments of the ion bulk velocity in the magnetosheath from the FPE instrument are underestimates as discussed above. The X fan plasma instrument on ISEE 1, on the other hand, can be used to detect relatively cold ion beams. Figure 8 is a plot of the plasma moments obtained from measurements of the ISEE 1 X fan detector during the hour of interest. It shows that the ion bulk velocity in the higher-density plasma of the magnetosheath is ~20% higher than what is calculated from the ISEE 2 FPE measurement. As the two spacecraft are separated by only ~200 km during this interval, one can use the ISEE 1 measurements (at lower temporal resolution) to characterize the magnetosheath flow speeds at ISEE 2. Figure 8

shows that the magnetosheath flow speed exceeds 600 km/s, with peak values of ~780 km/s. These flow speeds are comparable with those measured at IMP 8 in the dusk magnetosheath (see Figure 4). Thus on both flanks of the magnetosphere, the magnetosheath flow speeds exceeded the solar wind velocity.

IMP 8 on the duskside of the magnetosheath saw fluctuations of the magnetic field with periods of ~5 min (Figure 9). Since the time resolution of the plasma data is poor, we are unable to analyze the corresponding plasma fluctuations quantitatively, but it seems that IMP 8 always stayed in the magnetosheath during the interval of interest. However, we have compared power spectra of the field fluctuations at IMP 8 and ISEE 2 on the duskside and dawnside of the magnetopause, respectively, and we have found that they differ. Figure 10 shows the power spectra of three components and total strength of magnetic field fluctuations for the time interval of 1430–1540. There are peaks of power density at ISEE 2 near ~4 mHz whereas IMP 8 has a peak of lower frequency, ~3 mHz.

Table 1 summarizes the plasma properties observed in the solar wind and on the two flanks of the magnetosheath during the period from 1400 to 1800 UT. The solar wind velocity was 560 km/s, making a small angle with respect to the magnetotail axis, the ion temperature was of the order of 1 eV and the number density was 3 cm^{-3}. In the magnetosheath, the flow velocity was around 680 km/s and the flow angle was small but with large fluctuations ($\pm 5°$). The small flow angle in the magnetosheath indicates a very small flaring of the magnetopause. According to a velocity calibration between the MIT plasma instruments on IMP 7 and those on IMP 8, the magnetosheath flow velocity measurements might differ by $\lesssim 10\%$. The evidence of higher flow velocity in the magnetosheath is significant.

The dayside magnetopause has been described as a multilayered structure in several studies [*Sckopke et al.*, 1981; *Paschmann et al.*, 1982; *Sibeck et al.*, 1990; *Song et al.*, 1990*a*]. The complexity of the plasma and field structure of the interface between the solar wind and the magnetosphere on the dayside should have some relation to the boundary structure in the tail. Thus, it is meaningful to compare our complicated boundary crossings with those found on the dayside. Table 2 lists a comparison of our event with an event observed by ISEE on November 6, 1977, during which the IMF had a large B_y and a small but variable B_z component. *Sckopke et al.* [1981] found that two different layers, the boundary layer proper and the halo, could be classified. For the same event, *Paschmann et al.* [1982] described the structure as the boundary layer with flux transfer events (FTEs) and the halo. Later on, *Sibeck et al.* [1990] interpreted it as the plasma depletion layer and the LLBL. The halo of *Sckopke et al.* [1981] and *Paschmann et al.* [1982] (or the LLBL of *Sibeck et al.* [1990]) was a region of plasma transition between the magnetosheath and the magnetosphere and had the same magnetic field orientation as in the magnetosphere. A detailed discussion of the November 6 event can be found in the paper of *Sibeck et al.* [1990]. As a comparison, the LLBL of our event corresponds to some extent to the halo but an overwhelmingly tailward streaming plasma was seen (Figure 6). On the other hand, the boundary layer proper, the boundary layer of FTEs or the plasma depletion layer of these different studies had not only different plasma properties from those of the halo and the magnetosphere but also a complex magnetic field configuration. The magnetic field configuration of the event is so complex that the different analyses gave different physical explanations for the observations. For example, bipolar signatures of magnetic field were

attributed to the presence of FTEs by *Paschmann et al.* [1982], and a magnetic field draping effect at the magnetopause was interpreted as a result of a special magnetic field orientation in the depletion layer by *Sibeck et al.* [1990]. The magnetosheath of our event also had a complex magnetic field structure (Figure 6). As the IMF was strongly northward in our event, it seems unlikely that the FTEs discussed by *Paschmann et al.* [1982] are relevant to the interpretation of our boundary layers. And also because we do not have observations that show consistently a multilayered structure in the magnetosheath, we have not been able to determine whether or not the region we call the magnetosheath is the plasma depletion layer of *Sibeck et al.* [1990].

Song et al. [1990*a*] proposed that three layers can be found at the boundary during northward IMF: the inner and outer boundary layers, and the magnetosheath transition layer. In our study, we have simply interpreted the boundary crossings as excursions between two different plasma regimes: the LLBL and the magnetosheath even though some of distributions in Figure 7 appear to be transitional. The region that we identify as the magnetosheath in our boundary layer crossings possibly includes the magnetosheath and the sheath transition layer of *Song et al.* [1990*b*]. The latter is, as mentioned, similar to the plasma depletion layer of *Zwan and Wolf* [1976] or *Sibeck et al.* [1990]. There is also a possibility that both the inner and the outer boundary of *Song et al.* [1990*a*] may apply to our LLBL. Nonetheless, because of the considerable inhomogeneity of plasma properties and magnetic field components in our crossings (Figures 6 and 7), the evidence seems insufficient for us to classify the boundary layers.

MODELS

Flow Acceleration in the Magnetosheath

Magnetosheath flows are often analyzed by use of gasdynamic models. In particular, the steady state gasdynamic model of *Spreiter et al.* [1966] provides useful profiles of plasma parameters throughout much of the magnetosheath. In the gas dynamic model, the fluid equations are solved without a magnetic field. After the flow field is determined, the magnetic fields are included by adding the solar wind field and mapping it into the magnetosheath by using the frozen-in field condition $\nabla \times (\mathbf{V} \times \mathbf{B}) = 0$, where $\mathbf{V}$ is the flow velocity vector and $\mathbf{B}$ is the magnetic field vector. The results of *Spreiter et al.* [1966] and *Spreiter and Alksne* [1969], and *Spreiter and Stahara* [1980] predict that the flow velocity in the magnetosheath never exceeds that of the upstream solar wind.

In regions of the magnetosheath where the magnetic energy density is low, the gasdynamic model is expected to provide an excellent approximation to the properties of the plasma. However, near the magnetopause where the normal component of the flow slows down, the magnetic field begins to become dynamically important [e.g., *Southwood and Kivelson*, 1992]. For example, the field may pile up and form the so-called depletion layer near the magnetopause [*Zwan and Wolf*, 1976; *Paschmann et al.*, 1978; *Crooker et al.*, 1979; *Sibeck et al.*, 1990] or slow mode-related structures may develop [*Song et al.*, 1990*b*]. In parts of the magnetosheath where the magnetic field is dynamically important, the gasdynamic model may give misleading results.

Phenomenologically, the solar wind plasma near the magnetopause of the Earth or the other planets acquires considerable inhomogeneity because it is confined to flux tubes that extend through the bow shock, linking the unperturbed solar wind at the ends to plasma that has been

diverted around the magnetopause. The consequences are most extreme for flux tubes that pass near the stagnation point and then flow antisunward very near the magnetopause. If a magnetic flux tube near the Sun-Earth line in the solar wind approaches the Earth, the portion of the flux tube near the subsolar point slows down across the bow shock, continues to slow as it approaches the magnetopause and then is diverted around the flanks of the magnetopause as part of the magnetosheath flow. The portions of a flux tube outside of the bow shock continue to move with the solar wind plasma. This means that magnetic tension $\mathbf{B}\cdot\nabla\mathbf{B}/4\pi$ builds up unless the flux tube reconnects with magnetospheric field lines. Figure 11 illustrates the magnetic field structure in the magnetosheath for a northward IMF if no reconnection occurs at the magnetopause. The argument is equally valid for any other direction of the IMF provided that magnetic reconnection is not overwhelmingly important. If the portions of magnetic flux tubes in the magnetosheath, especially the ones near the subsolar magnetopause, slow down in the vicinity of the subsolar point, they must speed up elsewhere to catch up with the ends that remain in the solar wind. Somewhere their flow velocity must exceed the solar wind speed. The question remaining is where do these flux tubes start to accelerate or, in other words, where does the magnetic tension in the flux tubes begin to release? As an analogy, the release of magnetic tension is like launching a stone from a slingshot. If there is no drag on the band, the stone will be launched and the tension of the band will be released. Around the dayside, the magnetopause provides the drag on the magnetic field in the magnetosheath. On the nightside flanks, the drag decreases and the tension is released. The shape of the magnetopause is important in controlling the drag, and pressure balance at the magnetopause is crucial.

To estimate quantitatively the importance of the magnetic field in the magnetosheath for the case of interest here, we use data from spacecraft observations. We introduce the steady state MHD equations in Gaussian units,

$$\nabla\cdot(\rho\mathbf{V}) = 0 \tag{1}$$

$$\rho\mathbf{V}\cdot\nabla\mathbf{V} = -\nabla\left(P+\frac{B^2}{8\pi}\right)+\frac{1}{4\pi}\mathbf{B}\cdot\nabla\mathbf{B} \tag{2}$$

$$\nabla\times(\mathbf{V}\times\mathbf{B}) = 0 \tag{3}$$

where ρ is the mass density and P is the thermal pressure of the fluid. Equation (3), in which we applied the Faraday's law and the frozen-in field condition, describes how the flow and the magnetic field are coupled. Equation (2) expresses the condition of force balance in the fluid. The model of *Spreiter et al.* [1966] sets $\mathbf{B} = 0$ in equation (2) and then solves for $\mathbf{B}$ using equation (3) after the flow field is obtained. This requires that the magnetic effects in equation (2) be small compared with the velocity dependent terms. To verify the validity of the approximation for the case of interest to us, we use the data from our spacecraft observations. Considering the force balance in the direction parallel to the x axis at $z \simeq 0$ and y = constant (Figure 12) and applying equation (1), equation (2) becomes

$$\frac{\partial}{\partial x}(\rho V_x^2) = -\frac{1}{8\pi}\frac{\partial B^2}{\partial x} - \frac{B^2}{4\pi R_C} \tag{4}$$

where we are assuming that for this event the thermal pressure P was small compared with the magnetic pressure in the inner magnetosheath. R_C is the radius of curvature of magnetic field lines. By integrating equation (4) from x_1 to x_2, we approximate the integral by

$$\rho_2 V_{x2}^2 - \rho_1 V_{x1}^2 \simeq -\frac{B_2^2 - B_1^2}{8\pi} - \frac{\Delta X}{8\pi}\left(\frac{B_2^2}{R_{C2}} + \frac{B_1^2}{R_{C1}}\right)$$

$$\simeq \frac{1}{8\pi}\left[B_1^2\left(1 + \frac{|\Delta X|}{R_{C1}}\right) - B_2^2\right] \tag{5}$$

where $\Delta X = x_2 - x_1 < 0$. The integral of the curvature term in equation (4) is performed by taking the average (1/2) of the sum of B^2/R_C at the beginning and the end of the integral path x_1 and x_2. We are assuming $R_{C2} \rightarrow \infty$ at $x = x_2$ where the magnetic tension is fully released. R_{C1} is of the order of the half size of the magnetopause. If we neglect the particle flux at $x = x_1$, which means $\rho_1 V_{x1}^2 \simeq 0$, and assume $\rho_2/\rho_1 = B_2/B_1$, equation (5) becomes

$$V_{x2}^2 = \frac{1}{2} V_{A1}^2 \left[r\left(1 + \frac{|\Delta X|}{R_{C1}}\right) - \frac{1}{r}\right] \tag{6}$$

where $V_{A1}^2 = B_1^2/(4\pi\rho_1)$ and $r = B_1/B_2 \geq 1$. Equation (6) shows that the flow acceleration is characterized by the Alfvén speed V_{AI}, the ratio of B_1/B_2, and the geometric factor $|\Delta X|/R_{C1}$. Figure 13 shows relations between V_{x2}/V_{A1} and r for different geometric factors. When $|\Delta X|/R_{C1} = 0$, the magnetic field lines are straight and acceleration is produced by the release of magnetic pressure. In our event, B_T is $\approx$ 40 nT (or 4×10^{-4} G) in the magnetosheath. We might assume that B_1 is $\gtrsim$ 40 nT, which is not unusually large for measurements near the subsolar magnetopause (see, for example, *Gosling et al.* [1986, 1991], *Sibeck et al.* [1990], and *Song et al.* [1990*a*]), and the number density is $\lesssim$ 3 cm^{-3}. The Alfvén speed V_{AI} is ~500 km/s. Assuming B_2 = 20 nT and $|\Delta X|/R_{C1} = 2$, the maximum velocity V_{x2} gained from the acceleration achieved from the magnetic field is $\sim 1.5 V_{AI}$ or 750 km/s (Figure 13). This estimate implies that the magnetic tension in the magnetosheath is significantly important in accelerating the magnetosheath plasma near the magnetopause.

Magnetopause Flaring

According to the spacecraft observations of the position of the magnetopause by *Petrinec et al.* [1991] for $X_{GSM} \gtrsim 0\ R_E$ and by *Sibeck et al.* [1991] for $X_{GSM} \gtrsim$ -20 R_E, the degree of flaring of the magnetopause depends upon the direction of the IMF. The flaring is greater for a southward IMF than for a northward IMF as a consequence of dayside reconnection [*Coroniti and Kennel*, 1972]. For a northward IMF, no reconnection should occur at low latitudes on the dayside magnetopause and therefore no magnetic flux should be added to the tail lobes. Nonreconnected flux tubes pile up near the subsolar magnetopause where they lose plasma [*Zwan and Wolf*, 1976; *Song et al.*, 1990*a, b*] and then begin moving further downstream along the magnetopause. In the immediate vicinity of the magnetopause, the magnetic pressure in the magnetosheath becomes important to the pressure balance between the magnetosheath plasma

and the tail magnetospheric plasma. As the data show (Figures 6 and 7*a*), not only are the variations of magnetic pressure, but not the thermal pressure, highly correlated with the boundary layer crossings but also the magnetic pressure dominates the thermal pressure. However, the total pressure remains unbalanced at the magnetopause with magnetosheath pressure dominant. It is possible that the plasma pressure in the LLBL was underestimated. Dynamic pressure does not contribute to pressure balance for the observed 0° flare. This appears to require reduction of the open flux in the tail.

Kelvin-Helmholtz Instability Generated
Boundary Layer Perturbations

As described in the introduction, the Kelvin-Helmholtz (K-H) instability occurs in regions where a velocity shear exists if the change of velocity across the gradient exceeds a critical velocity. The LLBL is a transitional region where the flow velocity changes from high in the magnetosheath to low in the plasma sheet. Our observations show a high-speed flow in the magnetosheath ($\gtrsim$650 km/s) and a strong velocity shear across the boundary with the LLBL. The phase delay of the magnetopause crossings between ISEE 1 and ISEE 2 is consistent with propagation antisolar. We then pursue the possibility that the waves seen by ISEE 2 (Figure 6) are K-H-generated waves. Schematically, Figure 14 shows the waves seen by ISEE 2 and IMP 8 on different sides of the magnetopause. It is an important issue in discussing waves generated by an instability to consider the growth rate of the waves. To estimate the growth rate of waves generated by the K-H instability, we make use of the work of *Miura and Pritchett* [1982] (see also, for example, *Pu and Kivelson* [1983] and *Ogilvie and Fitzenreiter* [1989]). For the case of the magnetic fields on two sides of the boundary parallel to one another, the maximum growth rate γ, satisfying $\gamma a/V_o \simeq 0.07$, occurs at $ka \simeq 0.6$ while the average fast magnetosonic Mach number of the plasma ($M_f = V_o/(C_S^2 + V_A^2)^{1/2}$) is $\sim$1.6, where V_o is the total jump of the velocity across the boundary, k is the wave number in the flow direction and a is the thickness of the boundary layer. Based on our observations, we put $V_o = 650$ km/s, the sound speed $C_S \simeq 120$ km/s (for an isotropic and adiabatic plasma with dominant ion temperature T_i = 100 eV) and the Alfvén speed $V_A \simeq 380$ km/s (with B = 30 nT and n_i = 3 cm^{-3}). The time lag of magnetic fluctuations (typically 0.65 s) between ISEE 1 and ISEE 2 at 1400 to 1800 UT gives a phase velocity of the magnetopause surface waves of $\sim$300 to 350 km/s and hence the wavelength is of the order of 15 R_E for the waves with 5-min period. This means $k = 2\pi/15\ R_E^{-1}$.

Surface waves on the dawnside of the magnetopause have been studied by *Sckopke et al.* [1981] at $\sim$0800 hours local time (LT) and by *Lepping and Burlaga* [1979] at $\sim$0600 LT. The reported waves had periods of the order of $\sim$2–5 and $\sim$2–4 min, respectively, and wavelengths of the order of $\sim$3–8 and $\sim$6–12 R_E, respectively. In comparison, the surface waves we found have periods of $\sim$5 min and wavelengths of $\sim$15 R_E. The result may indicate a local time dependence of wavelength: the wavelength of the observed surface wave at the magnetopause increases with the solar zenith angle. This might be explained as a result of the increase of magnetosheath flow velocity away from the subsolar point since the plasma at the leading portion of a wave moves faster than at the trailing portion. *Song et al.* [1988] examined surface waves with periods of 2 min or greater at the magnetopause. Their data covered a wide range of local time from noon to dawn or to dusk. They have found that the average

wave period (the average time per crossing, which is taken from $\bar{t}/\bar{n}$ in Table 1 of *Song et al.* [1988]) is 4.4±0.9 min for the northward IMF and is 5.3±0.5 min without considering the IMF dependence. From these studies, we may conclude that a characteristic period of surface waves at the magnetopause is of the order of 5 min.

The thickness of the boundary layer a can be inferred from the requirement (see above) [*Miura and Pritchett*, 1982] that the fastest growing mode satisfies $ka \simeq 0.6$ which implies that $a \simeq 1.5\ R_E$. The growth rate γ of the wave is $0.07\ V_o/a \simeq 4.8 \times 10^{-3}\ s^{-1}$. That means the wave with 5-min period grows in amplitude by $e^{4.8\times10^{-3}\times300}$, which is approximately equal to 4 times the initial amplitude within a wave cycle. These numbers imply that the K-H instability has reached the nonlinear regime. These estimates give us confidence that the waves at the magnetopause are likely to be K-H-generated waves. Since the properties of K-H waves depend on the local properties of the plasma and the thickness of boundary layer, we can understand why the wave frequency at IMP 8 differs somewhat from that measured at ISEE 2.

The shape of the surface waves at the magnetopause is studied by using a minimum variance analysis of the magnetic field measurements. The intervals of inbound and outbound magnetopause crossings of ISEE 2 were selected based on the properties of the plasma parameters and the magnetic field components. After dropping intervals for which there were ambiguities in finding the normal direction of the magnetopause, or, in other words, having no significantly small eigenvalues, we chose 37 outbound and 29 inbound crossings for a statistical analysis (Table 3). Since the result (Table 3) shows that the uncertainty of determining the normal direction of the magnetopause is large, we use these results merely to infer that ϕ^* was larger for outbound crossings than for inbound crossings. Relative to the average magnetopause, which makes an angle of ~3° with the aberrated X_{GSM} (Table 1), this leads to the conclusion that the surface is more rotated for outbound crossings than for inbound crossings. ISEE 2 (Figure 6) also measured particularly strong magnetic fluctuations, especially in the B_x component, during outbound crossings, which indicates either a stronger current density at the boundary or a faster pass through the boundary on outbound relative to inbound crossings.

Fairfield [1976] has studied surface waves at the flank magnetopause by using IMP 6 data at the time interval from 0800 to 1500 UT on August 28, 1971. He found that the angles between the Sun-Earth line and the normal of the magnetopause during outbound, from the magnetotail to the magnetosheath, and inbound crossings have medians at 81.6° and 87.4°, respectively. And the median for all crossings is 84.2°. He has concluded that the flaring of the magnetopause is around 6° away from the Sun-Earth line, which is reasonable if the shape of the waves is sinusoidal. Since he didn't discuss the average flow angle of the magnetosheath plasma just outside the magnetopause, the angle of tail flaring was not unambiguously decided and, therefore, the assumption of a sinusoidal wave structure was not necessarily true.

Figure 14 shows a schematic of a possible wave structure at the magnetopause that is consistent with our observations. The diagram is taken by cutting through a X-Y_{GSM} plane at a small but positive Z_{GSM} near where the ISEE spacecraft were located and letting the representative magnetic field lines go through the plane and extend to the positive Z_{GSM} domain. The current layer makes a larger angle with the direction of the average magnetosheath flow V_{Sheath} (ϕ in Table 1) at the outbound crossings and a smaller angle at the inbound crossings (ϕ^* in Table 3). The magnetic tension in the magnetosheath is strongest, or the field lines are

bent the most, close to the magnetopause. The inner sheath magnetic field lines have a negative B_x component (the field lines are tilted to the negative x direction near the ISEE path) and the outer sheath magnetic field lines have a positive one, which is consistent with the observations (Figure 6). Figure 14 also shows that the magnetic field in the magnetosheath drags the trailing edges of the waves toward the antisunward direction, which explains the sawtooth structure of the waves seen by ISEE (Figure 6 and Table 3).

THREE-DIMENSIONAL MHD SIMULATION

We have speculated that the acceleration of flow in the magnetosheath near the downstream magnetopause is caused by release of magnetic tension; this hypothesis is supported by results obtained by using the MHD code of *Ogino et al.* [1992]. Three runs with different IMF B_z (10, 0 and -10 nT) are examined. The upstream solar wind parameters are appropriate to the event being studied, with velocity V_{SW} = 600 km/s, ion temperature T_i = 2 eV, and ion number density N_i = 5 cm^{-3}. For these runs we used a 60x30x30 point grid with a grid spacing of 1 R_E. The simulation was run until the magnetic fields and the plasma parameters were changing slowly. For example, the magnetic field strength changed $\lesssim$0.5% and the velocity and density changed $\lesssim$1% in the 10 min prior to the step used to analyze the northward IMF case. We display the velocity and magnetic field data in a form suitable for comparison with our phenomenological model. Figure 15 shows the velocity contours in the magnetosheath for the different IMF B_z. Positions of the bow shock and the magnetopause (the heavy solid curves) for the three cases are drawn in all three panels. For a comparison, the position of magnetopause for IMF B_z = 10 nT is also overlaid on the panels of no IMF and IMF B_z = -10 nT (the heavy dashed curves). For the cases of no IMF and northward IMF, the magnetopause is defined as the boundary between field lines for which both ends emerge through the boundary of the simulation volume (which represent solar wind field lines unconnected to the Earth) and those that do not. For the case of southward IMF, the magnetopause is defined as the position of the current layer (maximum $\nabla \cdot B_z$). For the cases of southward IMF and no IMF (Figures 15*a* and 15*b*), the magnetopause is more flared than it is for the northward IMF case (Figure 15*c*). Near the downstream position of ISEE 2 (IMP 8) the simulation for negative IMF B_z gives $|\phi| \simeq 11^\circ$. These angles can be compared with the flaring angles observed during hours 0900–1100 UT when $B_z < 0$ in the IMF can be inferred from IMP 8. The observed flaring angles $\phi \simeq 10^\circ$ at IMP 8 are close to the model values. For northward IMF, the flaring is close to $\phi \simeq 0^\circ$ at the ISEE 2 and IMP 8 positions, also consistent with observations. The velocity for the northward IMF case starts to exceed the upstream solar wind velocity near X_{GSM} = -10 R_E in the magnetosheath. Neither of the other cases develops flows faster than the upstream flow in the magnetosheath within the simulation box.

To verify if the magnetic tension in the magnetosheath is important in accelerating plasma, we trace the magnetic field lines along the flow path through the region of accelerated flow. The light curve near the magnetopause in Figure 15*c* is the path that we follow. Figure 16 shows the magnetic field lines that cross the equator along the designated curve. In Figure 16, the magnetic field lines near the magnetopause stagnation point begin to bend downstream. The bending grows as they slip around the dayside. As they approach the terminator, the field lines begin to straighten just where the magnetic tension $\mathbf{B}\cdot\nabla\mathbf{B}/4\pi$ releases its energy to the plasma.

In order to catch up with the solar wind plasma, the plasma on the part of the magnetic flux tubes in the magnetosheath must be flowing faster than the solar wind.

We noticed in the previous section that the position where the magnetic flux starts to release the tension depends on the shape of the magnetopause. And we declared that the acceleration is more likely to happen when the flaring of the magnetopause is small. The simulation result supports our model (Figure 15*c*). In summary, the result of a three-dimensional simulation indicates a significant magnetic effect not only on the flow velocity of the magnetosheath plasma but also on the shape of the magnetopause.

DISCUSSION AND SUMMARY

We have found that magnetic effects are important in controlling the plasma flow velocity in the magnetosheath near to the magnetopause boundary. Observationally, one often sees high-speed flows in the magnetosphere near the magnetopause which can be attributed to magnetic reconnection, but such events do not show accelerated flows in the magnetosheath [e.g., *Gosling et al.,* 1986]. Our study brings up a possibility that the plasma near, but external, to the magnetopause can be accelerated by magnetic tension on one side of the boundary or the other; this means that neither reconnection nor merging processes are needed to account for the flow acceleration.

Although, in this study, we proposed an acceleration mechanism only for a special IMF condition (strongly northward), other IMF directions can build up magnetic tension in the magnetosheath if the magnetic field lines hang up at the magnetopause and no reconnection occurs. For the normal spiral angle of the IMF, the accelerated flows would be expected at the high-latitude magnetopause in both hemispheres. The process requires that the magnetic tension be strong enough to make the $\mathbf{B}\cdot\nabla\mathbf{B}/4\pi$ term in the equation of motion dominant.

It is also interesting how the shape of the magnetopause changes with northward IMF. *Sibeck et al.* [1991] reported that for a northward IMF the position of the subsolar magnetopause moves out as the IMF B_z increases. In our study, the magnetopause has been found to have stopped flaring at $X_{GSM} \simeq$ -15 R_E. The dotted curve in Figure 1 shows the position of the magnetopause observed in our event. The boundary, less flared than the nominal magnetopause, has been drawn to show the ISEE 1 and 2 spacecraft just at the boundary and symmetric about an aberrated axis. The symmetric assumption is dictated by the evidence from IMP 7 that the solar wind flow was nearly radial. The model leaves IMP 8 in the magnetosheath, which is consistent with the data. The dotted curve has also been closed across the aberrated axis at a position sunward of the nominal nose of the magnetopause. Although this outward extension near noon has not been observationally proved for our event, it is consistent with Sibeck et al.'s statistical results described above.

We propose that the magnetopause shape shown in Figure 1 can be interpreted as follows: The decreased flaring of the magnetopause in the presence of prolonged northward IMF is consistent with a decrease of magnetic flux in the tail lobes. To some extent the decreased tail flux implies a decrease in the amount of open flux in the magnetosphere and corresponds to the decreased polar cap area found for northward IMF B_z. A decrease in open flux in the tail necessarily implies an increase in the flux on the dayside magnetosphere. However, one needs also to recognize that high-latitude reconnection can shift open field lines from the tail

to the dayside without changing the polar cap flux. The reason is that the lobe field lines at the high-latitude reconnection sites poleward of the cusp are removed by solar wind flow after reconnection and this decreases the magnetic flux in the tail lobes. On the other hand, the low-latitude ends of the reconnected lobe field lines drape from the polar cusps across the dayside, thereby adding magnetic flux to the dayside magnetosphere. If the strength of the magnetic field in the dayside magnetosphere does not increase much but balances the pressure of the magnetosheath, the subsolar magnetopause must move out. To estimate the change of the standoff distance with the size of the tail cross section, we map the polar cap to the dayside equatorial plane using a dipole field. Assuming that a fraction f of the magnetic flux of the polar cap Φ_{PC} is added to the dayside magnetosphere both from a reduction in the net open flux and from lobe reconnection, and that the average sizes of the polar cap and of the dayside magnetopause are $\sim 15°$ and L (in Earth radii, R_E), respectively, we have

$$f\Phi_{PC} \simeq \pi f\,(2B_o)\; R_E^2\; \sin^2 15° \simeq 2\pi\, L\, \Delta L \frac{B_o}{L^3} R_E^2 \tag{7}$$

where B_o is the magnetic field strength at the equator on the surface of the Earth. If the average standoff distance of the subsolar magnetopause L is 10 R_E, the change of the standoff distance is

$$\Delta L = f\, L^2\, \sin^2 15° \simeq 6.7f \tag{8}$$

This shows that as the magnetic flux in the magnetotail decreases by, for example, a factor of f = 1/7 (or the radius of the tail decreases by 5% if the magnetic field strength in the tail lobes does not change very much but balances that in the tail magnetosheath), the standoff distance L increases by ΔL = 1 R_E, which is comparable with the displacement observed by *Sibeck et al.* [1991].

It is natural to ask why accelerated flows of the sort we report, quite different in character from those associated with reconnection on the flanks, have not been identified previously. We think that the explanation relates to the relatively infrequent occurrence of persistent northward IMF, the fact that most of the high-resolution plasma data comes from spacecraft in relatively low inclination orbits, and the scarcity of multispacecraft observations. At high-latitude magnetopause crossings, one might expect to encounter flows accelerated by field line tension when the IMF lies close to the ecliptic plane, and this would be interesting to look for in HEOS data.

A complete MHD flow model needs to be worked out explicitly. More observations of high-speed flows in the magnetosheath are necessary to verify the importance of the magnetic tension for different orientations of the IMF. Since it is hard to estimate the magnetic tension directly from observations, three-dimensional MHD simulations will help us to identify the role of the magnetic field in the magnetosheath.

We summarize the principal points of our study: (1) We have presented evidence of high-speed flows ($V > V_{SW}$) in the low-latitude magnetosheath during a strongly northward IMF. (2) Magnetic tension in the magnetosheath and the geometry of the magnetopause both play important roles in accelerating plasmas in the magnetosheath. (3) Anomalous perturbations

at the magnetopause were probably the consequence of the K-H instability. (4) Results of a three-dimensional MHD simulation support the phenomenological model. (5) According to our prediction, the standoff distance of the subsolar magnetopause is possibly larger during stronger northward IMF.

Note that while this paper was being typeset, we found that the magnetopause crossing on February 15, 1978, has been previously analyzed by *Couzens et al.* [1985]. They mainly used energetic particle data from the ISEE spacecraft and concentrated on estimates of the velocity and of the shape of the surface waves. They concluded that waves in the interval from 1400 to 1800 UT were mainly sinusoidal which is different from our result.

Acknowledgments. We thank C.T. Russell for supplying the ISEE magnetometer data. We thank Tatsuki Ogino for letting us use his global MHD simulation code. We also thank Tim Eastman and M.A. Saunders for extremely useful conversations regarding properties of magnetospheric boundary layers. Computing resources were supplied both by the Institute of Geophysics and Planetary Physics and the Department of Earth and Space Sciences of UCLA. The work was supported by the National Aeronautics and Space Administration under grant NAG 5–1529 and by the Division of Atmospheric Sciences of the National Science Foundation under grant ATM 91–15557. Work at Los Alamos was performed under the auspices of the U.S. Department of Energy with support from NASA under grant 5–04039–D. The simulation was performed with support from the Space Physics Theory Program under grant NAG 1480. UCLA IGPP publication 3696.

The editor thanks K. W. Ogilvie and K. Takahashi for their assistance in evaluating this paper.

REFERENCES

Axford, W. I., Viscous interaction between the solar wind and the Earth's magnetosphere, *Planet. Space Sci., 12*, 45, 1964.

Axford, W. I., and C. O. Hines, A unifying theory of high-latitude geophysical phenomena and geomagnetic storms, *Can. J. Phys., 39*, 1433, 1961.

Bame, S. J., J. R. Asbridge, H. E. Felthauser, E. W. Hones, and I. B. Strong, Characteristics of the plasma sheet in the Earth's magnetotail, *J. Geophys. Res., 72*, 113, 1967.

Bame, S. J., J. R. Asbridge, H. E. Felthauser, J. P. Glore, G. Paschmann, P. Hemmerich, K. Lehmann, and H. Rosenbauer, ISEE-1 and ISEE-2 fast plasma experiment and the ISEE-1 solar wind experiment, *IEEE Trans. Geosci. Electron., GE-16*, 216, 1978.

Coroniti, F. V., and C. F. Kennel, Changes in magnetospheric configuration during the substorm growth phase, *J. Geophys. Res., 77*, 3361, 1972.

Couzens, D. A., G. K. Parks, K. A. Anderson, R. P. Lin, and H. Reme, ISEE particle observations of surface waves at the magnetopause, *J. Geophys. Res., 90*, 6343, 1985.

Crooker, N. U., T. E. Eastman, and G. S. Stiles, Observations of plasma depletion in the magnetosheath at the dayside magnetopause, *J. Geophys. Res., 84*, 869, 1979.

Dungey, J. W., Interplanetary magnetic field and the auroral zones, *Phys. Rev. Lett., 6*, 47, 1961.

Fairfield, D. H., Waves in the vicinity of the magnetopause, in *Magnetospheric Particles and Fields*, edited by B. M. McCormac, pp. 67–77, D. Reidel, Norwell, Mass., 1976.

Farris, M. H., S. M. Petrinec and C. T. Russell, The thickness of the magnetosheath: Constraints on the polytropic index, *Geophys. Res. Lett., 18*, 1821, 1991.

Gosling, J. T., M. F. Thomsen, and S. J. Bame, Accelerated plasma flows at the near-tail magnetopause, *J. Geophys. Res., 91*, 3029, 1986.

Gosling, J. T., M. F. Thomsen, S. J. Bame, R. C. Elphic, and C. T. Russell, Observations of reconnection of interplanetary and lobe magnetic field lines at the high-latitude magnetopause, *J. Geophys. Res., 96*, 14,097, 1991.

Howe, H. C., Jr., and J. H. Binsack, Explorer 33 and 35 plasma observations of magnetosheath flow, *J. Geophys. Res., 77*, 3334, 1972.

Lepping, R. P., and L. F. Burlaga, Geomagnetopause surface fluctuations observed by Voyager 1, *J. Geophys. Res., 84*, 7099, 1979.

Miura, A., and P. L. Pritchett, Nonlocal stability analysis of the MHD Kelvin-Helmholtz instability in a compressible plasma, *J. Geophys. Res., 87*, 7431, 1982.

Ogilvie, K. W., and R. J. Fitzenreiter, The Kelvin-Helmholtz instability at the magnetopause and inner boundary layer surface, *J. Geophys. Res., 94*, 15,113, 1989.

Ogilvie, K. W., R. J. Fitzenreiter, and J. D. Scudder, Observations of electron beams in the low-latitude boundary layer, *J. Geophys. Res., 89*, 10,723, 1984.

Ogino, T., R. J. Walker, and M. Ashour-Abdalla, A global magnetohydrodynamic simulation of the magnetosheath and magnetosphere when interplanetary magnetic field is northward, *IEEE Trans. Plasma Sci.*, in press, 1992.

Paschmann, G., N. Sckopke, G. Haerendel, J. Papamastorakis, S. J. Bame, J. R. Asbridge, J. T. Gosling, E. W. Hones, Jr., and E. R. Tech, ISEE plasma observations near the subsolar magnetopause, *Space Sci. Rev.*, *22*, 717, 1978.
Paschmann, G., G. Haerendel, J. Papamastorakis, N. Sckopke, S. J. Bame, J. T. Gosling, and C. T. Russell, Plasma and magnetic field characteristics of magnetic flux transfer events, *J. Geophys. Res.*, *87*, 2159, 1982.
Petrinec, S. P., P. Song, and C. T. Russell, Solar cycle variations in the size and shape of the magnetopause, *J. Geophys. Res.*, *96*, 7893, 1991.
Pu, Z.-Y., and M. G. Kivelson, Kelvin-Helmholtz instability at the magnetopause: Solution for compressible plasma, *J. Geophys. Res.*, *88*, 841, 1983.
Russell, C. T., The ISEE 1 and 2 fluxgate magnetometers, *IEEE Trans. Geosci. Electron.*, *GE-16*, 239, 1978.
Saunders, M. A., Magnetosheath, magnetopause and low latitude boundary layer research, 1987–1989, *J. Atmos. Terr. Phys.*, *52*, 1107, 1990.
Sckopke, N., G. Paschmann, G. Haerendel, B. U. Ö. Sonnerup, S. J. Bame, T. G. Forbes, E. W. Hones, Jr., and C. T. Russell, Structure of the low-latitude boundary layer, *J. Geophys. Res.*, *86*, 2099, 1981.
Sibeck, D. G., R. P. Lepping, and A. J. Lazarus, Magnetic field line draping in the plasma depletion layer, *J. Geophys. Res.*, *95*, 2433, 1990.
Sibeck, D. G., R. E. Lopez, and E. C. Roelof, Solar wind control of the magnetopause shape, location, and motion, *J. Geophys. Res.*, *96*, 5489, 1991.
Song, P., R. C. Elphic, and C. T. Russell, ISEE 1 & 2 observations of the oscillating magnetopause, *Geophys. Res. Lett.*, *15*, 744, 1988.
Song, P., R. C. Elphic, C. T. Russell, J. T. Gosling, and C. A. Cattell, Structure and properties of the subsolar magnetopause for northward IMF: ISEE observation, *J. Geophys. Res.*, *95*, 6375, 1990*a*.
Song, P., C. T. Russell, J. T. Gosling, M. Thomsen, and R. C. Elphic, Observations of the density profile in the magnetosheath near the stagnation streamline, *Geophys. Res. Lett.*, *17*, 2035, 1990*b*.
Southwood, D. J., and M. G. Kivelson, On the form of the flow in the magnetosheath, *J. Geophys. Res.*, *97*, 2873, 1992.
Spreiter, J. R., and A. Y. Alksne, Plasma flow around the magnetosphere, *Rev. Geophys.*, *7*, 11, 1969.
Spreiter, J. R., and S. S. Stahara, Solar wind flow past Venus: Theory and comparisons, *J. Geophys. Res.*, *85*, 7715, 1980.
Spreiter, J. R., A. L. Summers, and A. Y. Alksne, Hydromagnetic flow around the magnetosphere, *Planet. Space Sci.*, *14*, 223, 1966.
Takahashi, K., D. G. Sibeck, P. T. Newell, and H. E. Spence, ULF waves in the low-latitude boundary layer and their relationship to magnetospheric pulsations: A multisatellite observation, *J. Geophys. Res.*, *96*, 9503, 1991.
Zwan, B. J., and R. A. Wolf, Depletion of solar wind plasma near a planetary boundary, *J. Geophys. Res.*, *81*, 1636, 1976.

S.-H. Chen, M. G. Kivelson, and R. J. Walker, Institute of Geophysics and Planetary Physics, University of California, 405 Hilgard Avenue, Los Angeles, CA 90024.
J. T. Gosling, Los Alamos National Laboratory, Los Alamos, NM 87545.
A. J. Lazarus, Center for Space Research, Department of Physics, Massachusetts Institute of Technology, Cambridge, MA 02139.

(Received May 29, 1992;
revised September 14, 1992;
accepted September 15, 1992.)

[1]Institute of Geophysics and Planetary Physics, University of California, Los Angeles.
[2]Also at Department of Earth and Space Sciences, University of California, Los Angeles.
[3]Los Alamos National Laboratory, Los Alamos, New Mexico.
[4]Center for Space Research, Department of Physics, Massachusetts Institute of Technology, Cambridge.

Paper number 92JA022630.
0148–0227/93/92JA-022630$05.00

CHEN ET AL.: MAGNETOSHEATH FLOWS AND BOUNDARY PERTURBATIONS

Fig. 1. Positions of the spacecraft ISEE 1 and 2, IMP 7 and IMP 8 at 1600 UT, February 15, 1978. Models of the bow shock [*Sibeck et al.*, 1991; *Howe and Binsack*, 1972] and magnetopause [*Farris et al.*, 1991; *Howe and Binsack*, 1972] are plotted. The dynamic pressure in the upstream solar wind for the models is ~2 nPa without considering the IMF B_z contribution. The dotted curve is a possible magnetopause for our event, obtained by extrapolating Sibeck et al.'s B_z dependent model subsolar and dawn-dusk distances to IMF $B_z \simeq 10$ nT and combining this with the observed magnetopause position from ISEE 2 by using a rescaled Howe and Binsack nightside magnetopause model. We have assumed symmetry about the aberrated X_{GSM} axis. The fact that IMP 8 was simultaneously in the magnetosheath on the duskside suggests that our model is not far off. The magnetopause crossings of ISEE 1 and 2 were identified by using ion and electron distribution functions and magnetic field components. The bow shock is represented for a nominal solar wind magnetic field of the order of 5 nT. The bow shock can be expected to have been further from the Earth and to have been more flaring in our event which probably had a smaller Mach number in the upstream solar wind as we believe the IMF was unusually large.

Fig. 2*a*. Data from the IMP 7 Los Alamos National Laboratory plasma instrument in the upstream solar wind. From top to bottom, the components are the ion bulk flow velocity, the azimuthal flow angle, the ion density, and the parallel and perpendicular ion temperatures. The azimuthal flow angle is zero antisunward and positive from dawn to dusk. Note that the azimuthal flow angle is the actual flow angle. The flow aberration due to the motion of the Earth's inertial frame with respect to Sun has been already removed.

Fig. 2*b*. Data from the MIT plasma instrument on IMP 7 in the upstream solar wind. From top to bottom, the components are ion bulk flow velocity, flow angles, ion number density, and ion temperature. Note that the azimuthal (east-west) flow angle is the actual flow angle (see Figure 2*a*). The MIT and the LANL instruments show that the average temperatures in the solar wind between 1400 and 1800 UT were ~5 eV and 1 eV, respectively, the number density was ~3 cm^{-3}, and the ion bulk flow velocity was 560 km/s. Since the flow angles measured by the two instruments are different, the flow direction of the solar wind remains indeterminate.

Fig. 3. A 24-hour overview plot of data from the magnetometer and the Fast Plasma Experiment on ISEE 2 on February 15, 1978. The auroral electrojet index AL is provided as an indicator of substorm activity. From top to bottom, the components are ion bulk flow velocity V_b, east-west flow angle ϕ (zero toward 0000 UT and positive from dawn to dusk), ion number density N_i, ion temperature T_i, magnetic field strength B_t and the AL index. Based on the plasma properties and the magnetic field strength, data segments are classified and labeled as follows: 1, plasma sheet; 2, magnetosheath; 3, lobe or plasma mantle; 4, magnetosheath; 5, plasma sheet; 6, LLBL or magnetosheath; and 7, a region of transition from LLBL to plasma sheet. The horizontal line segment across the sixth segment in the top panel is the averaged upstream solar wind velocity seen by IMP 7.

Fig. 4. IMP 8 plasma data for the same time interval as Figures 2 and 3. The vertical dashed lines correspond to the sixth data segment in Figure 3. The components are ion bulk flow velocity in kilometers per second, flow angles θ and ϕ in degrees, ion number density in cm^{-3} and ion temperature in electron volts. Note that θ=0 and ϕ=0 is purely antisunward, and θ and ϕ are positive northward and eastward, respectively. The marked change of plasma properties after 1400 UT was likely due to a change of upstream solar wind conditions. The temperature, especially after 1400 UT, is substantially lower than a typical sheath temperature, which is ~100 eV. The horizontal line segment in the top panel is the averaged upstream solar wind velocity seen by IMP 7.

Fig. 5. The magnetic field components measured at (top) ISEE 2 and (bottom) IMP 8 in GSM coordinates. The vertical dashed lines are the same as the ones in Figure 3. Note that ISEE 2 was crossing between different plasma regions and that IMP 8 remained in the magnetosheath. Lacking magnetic field observations in the upstream solar wind, we use the IMP 8 magnetometer as an indicator of IMF B_z. Corrections need to be made for the distortion of the IMF in the magnetosheath flow, but at low latitudes, such distortion affects predominantly the x and y components, and in the interval of primary interest (1400–1800 UT), these components are small. Referring to the second panel from the bottom, the IMF B_z changed sign several times and then at 0900 UT took on a steady value. After the IMF became strongly southward at 0900 UT, dayside reconnection presumably began and the magnetopause began to flare which caused the ISEE 2 spacecraft to enter the lobe (the third interval in Figure 3). After 1140 UT, the IMF turned strongly northward and this configuration lasted for many hours.

Fig. 6. An interval of ISEE 2 FPE and magnetometer data. The top four panels give the ion moments. The azimuthal flow angle ϕ is zero antisunward and positive from dawn to dusk. The bottom four panels are the magnetic field components in *GSM* coordinates and the total magnetic field strength. The vertical dashed lines separate the quasi-periodic structures. Each subinterval is considered to contain a complete cycle of crossing between the magnetosheath and the LLBL. The average upstream solar wind velocity (V_{sw}=560 km/s) seen by IMP 7 is overlaid on the V_b trace.

Fig. 7*a*. A 10-min interval of FPE and magnetometer data as a guide to the ion and electron distribution functions in Figure 7*b*. Six distinct electron and ion distribution functions were selected from a full cycle of plasma and field fluctuations. These data reveal the changes within a cycle as crossings of the magnetopause back and forth between the magnetosheath and the LLBL. The triangles in the N_i and B_x panels show the times when the measurements of Figure 7*b* were taken. The time resolution of the data is 12 s.

Fig. 7*b*. Selected electron and ion distribution functions at different positions of LLBL and in the magnetosheath. In each column, electron distributions are to the left and ion distributions are to the right. The FPE instrument made a measurement every 12 s and took ~3 s to collect data. The magnetic field projections on the X-Y_{SC} plane are drawn on top of the electron contours. The Sun is to the left and dusk is down. The LLBL is identified by the presence of cold streaming electrons along field lines and enhanced electron and ion temperatures. The magnetosheath is cold and shows no streaming along B. The labels at the top left corner of the electron contour plots correspond to the measurements labeled by numbered triangles in Figure 7*a*. The contours are classified as follows: 1 and 6 are the LLBL, 4 is the magnetosheath, and 2, 3, and 5 are the transitional regions between the LLBL and the magnetosheath.

Fig. 8. Data from the cross fan plasma instrument of ISEE 1. From top to bottom, the components are ion bulk velocity, azimuthal flow angles, ion number density and ion temperature. Note that the measured ion bulk flow velocity is different from that calculated from the FPE measurement on ISEE 2 (Figure 6).

Fig. 9. A 1-hour interval of IMP 8 plasma and magnetic field components to show the details of plasma and magnetic field perturbations at the duskside flank. The data show 5-min period fluctuations in magnetic field components. Because of the limited time resolution of the plasma instrument, the relation between the plasma and the magnetic field components is not clear. Note that the period of the magnetic fluctuations is not exactly the same as what ISEE 1 and 2 observed.

Fig. 10. Power spectra of three components and total magnetic fluctuations at interval of 1430–1540 UT, February 15, 1978, for ISEE 2 (the heavy curves) and for IMP 8 (the light curves). The Nyquist frequencies are 0.125 and 0.0327 Hz for ISEE 2 and IMP 8, respectively. The bandwidth is 5 for both spacecraft. Note that the major peaks of the spectra for ISEE 2 and IMP 8 are located at ~4 and ~3 mHz, respectively.

Fig. 11. A schematic diagram to illustrate a draping configuration of the IMF near the magnetopause. The diagram shows magnetic field lines in the magnetosheath near the magnetopause for a northward IMF. Field line bending develops as the flux tubes flow around the dayside magnetopause. Along the flanks, the release of magnetic tension of draped magnetic fields is proposed as an important mechanism for accelerating plasmas in the antisolar magnetosheath.

Fig. 12. A schematic diagram to illustrate a two-dimensional acceleration mechanism achieved by the magnetic field. The solid curves with arrows indicate magnetic fields. The open arrows indicate the flow velocity. R_C is the radius of curvature of magnetic field lines. At $x = X_1$ the magnetic tension (the dashed arrows) is maximum and the flow velocity is minimum. At $x = X_2$, the tension is minimum and the velocity is maximum.

Fig. 13. A family of solutions to equation (6). The diagram shows relations between V_{X2}/V_{A1} and B_1/B_2 for different geometric factors $\Delta X/R_{C1}$.

Fig. 14. A schematic diagram of the structure of the waves at the magnetopause. The diagram is taken by cutting through a X-Y_{GSM} plane at a small but positive Z_{GSM} by where ISEE spacecraft were passing and letting the representative magnetic field lines go through the plane and extend to the positive Z_{GSM} domain. Note that the magnetic tension is stronger at the inner part of the magnetosheath than at the outer part. The inner part of the magnetic field lines has a negative B_x component and the outer part has a positive one. The inner part of the magnetic field lines tends to come together at the outbound edges in the magnetosheath because of the magnetic tension.

Fig. 15. Velocity contours of a three-dimensional MHD simulation for different IMF conditions: (*a*) B_z=-10 nT, (*b*) no IMF, and (*c*) B_z=10 nT. The upstream solar wind is taken to have V_{SW} = 600 km/s, T_i = 2 eV, and N_i = 5 cm^{-3}. Positions of the bow shock and the magnetopause for three cases are drawn on to the plots (heavy curves). For a comparison, the magnetopause for B_z=10 nT is overlaid with Figures 15*a* and 15*b* (the dashed curves). The light curve near the magnetopause in Figure 15*c* is the path along which we trace magnetic field lines in the following diagram (Figure 16). The interval of the contours is 15 km/s. The portions of the dense and irrelevant contours inside the magnetopause and near the subsolar region are abbreviated. Note that a portion of flow velocity in the magnetosheath for the northward

IMF case (the stippled area) has a larger velocity than the upstream solar wind velocity (600 km/s).

Fig. 16. Magnetic field lines of the computer simulation with the IMF B_z = 10 nT that intersect the light curve in Figure 15*c*. The curvature of these field lines causes the plasma to be accelerated.

TABLE 1. Comparison of Plasma Parameters in the Solar Wind and in the Magnetosheath

	Solar Wind		Magnetosheath	
	IMP 7*	IMP 7†	IMP 8‡	ISEE 1§
V_b, km/s	560 ±8	550	683 ±49	667 ±35
ϕ, deg	-1.2 ±0.7	2.5	-1.7 ±5.2	3.0 ±5.3
T_i, eV	1.0 ±0.2	5	46 ±10	158 ±59
N_i, cm^{-3}	3.1 ±0.8	3	3.5 ±0.8	2.7 ±0.5

Time interval: 1400-1800 UT, February 15, 1978. Angle ϕ is positive from west to east. The solar wind aberration was corrected.
*LANL (37 points).
†MIT (estimate).
‡MIT (100 points).
§X fan (V_b>600, 120 points).

TABLE 2. Comparison of Two ISEE Magnetopause Crossings

	Further in	Inner	Outer	Further out
		*February 15, 1978, 1140-1800 UT**		
N_i, cm^{-3}	0.4	0.5	2	4†
T_i, keV	2	1	0.2	0.05†
V_b, km/s	$\lesssim$ 400 tailward and $\lesssim$ 200 sunward	250-600 tailward	550-700 tailward	650-800† tailward
$\mathbf{B}_{GSM}$ field, nT	(20, 10, 20); 30	(10, 5, 30); 32	(5, 5, 40); 41	(8, -4, 28); 29†
Classification of this paper	plasma sheet	LLBL	magnetosheath/ depletion layer	magnetosheath
		November 6, 1977, 0455-0555 UT‡		
N_i, cm^{-3}	1	2-3	10-14	30
T_i, keV	2	0.2-0.25	0.1-0.25	0.1
V_b, km/s	<50 undetermined	50 tailward and sunward	150-250 tailward	200 tailward
$\mathbf{B}_{GSM}$ field, nT	(-18, 16, 21); 32	(-20, 10, 25); 34	(-28, 5, 35); 45	(20, 23, -1); 31
Classifications				
Sckopke et al. [1981]	magnetosphere	halo	boundary layer proper	magnetosheath
Paschmann et al. [1978]	magnetosphere	halo	FTE	magnetosheath
Sibeck et al. [1990]	magnetosphere	LLBL	depletion layer	magnetosheath

*IMF: constantly strong northward. The position of ISEE was at 0300 LT and 10° above the X-Y_{GSM} plane.
†From IMP 8 at the dusk flank.
‡Adopted from *Sibeck et al.* [1990]. IMF: horizontal; mainly in B_y (GSM). B_z was small and changing sign. The position of ISEE was at 0800 LT and 30° above the X-Y_{GSM} plane.

TABLE 3. Statistics of Magnetopause Boundary Normal

		Outbound	Inbound
	Total	37	29
$\hat{n}$	ϕ^*, deg	-20 ± 16	-3 ± 19
	θ, deg	6 ± 27	8 ± 21

Time interval: 1400-1800 UT, February 15, 1978. The coordinate of the magnetopause boudnary normals $\hat{n}$ consists of the azimuthal angle ϕ^* (zero toward dawn; positive antisunward) and the elevation angle θ (zero at the equatorial plane; positive from south to north).

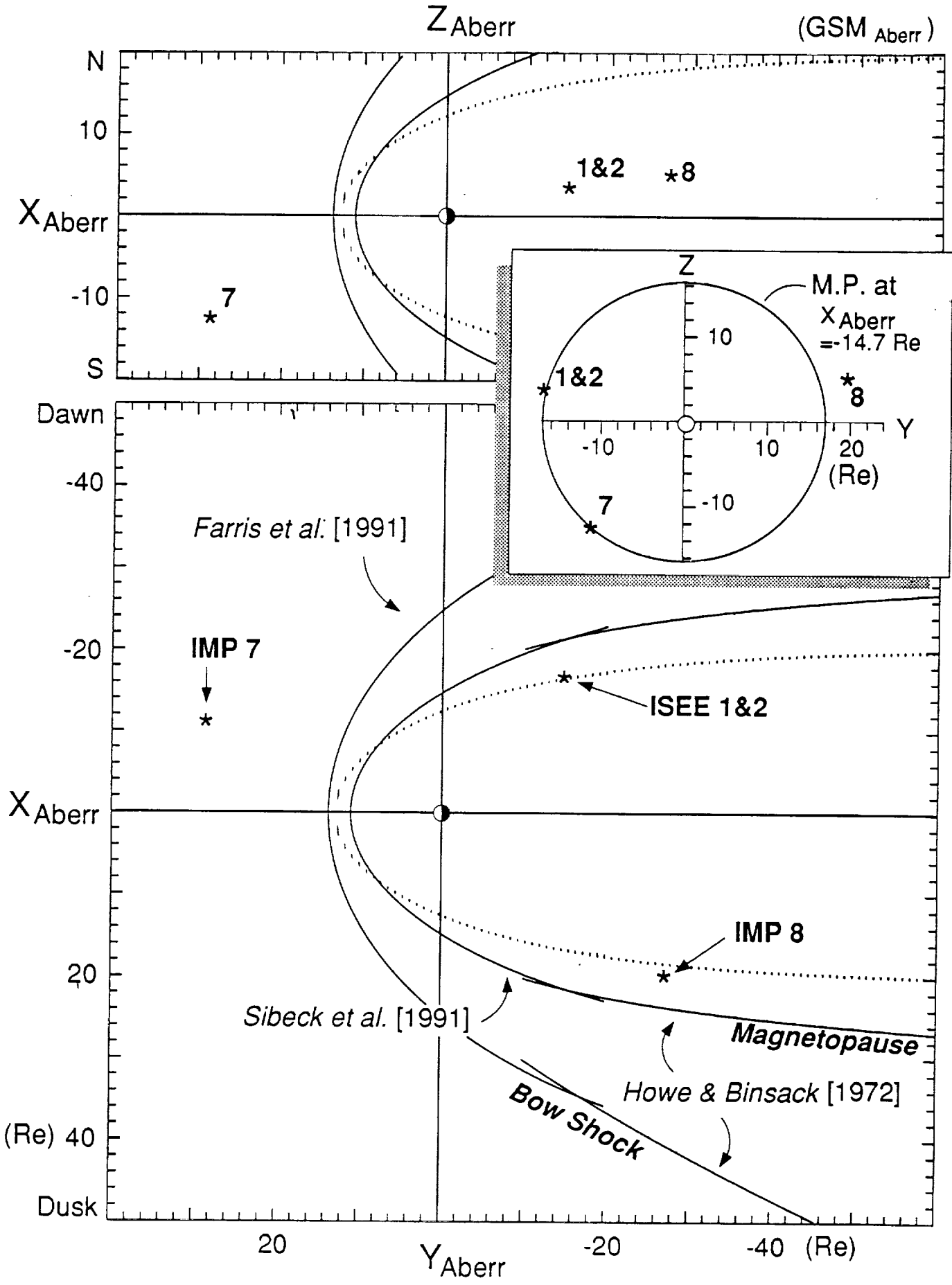
Z Aberr
(GSM Aberr)
N
10
X Aberr
-10
S
1&2
8
7
Z
M.P. at
X Aberr
=-14.7 Re
10
1&2
8
Y
-10
10
20
(Re)
7
-10
Dawn
-40
Farris et al. [1991]
IMP 7
-20
ISEE 1&2
X Aberr
IMP 8
20
Sibeck et al. [1991]
Magnetopause
Howe & Binsack [1972]
Bow Shock
(Re) 40
Dusk
20
Y Aberr
-20
-40 (Re)

Figure 1

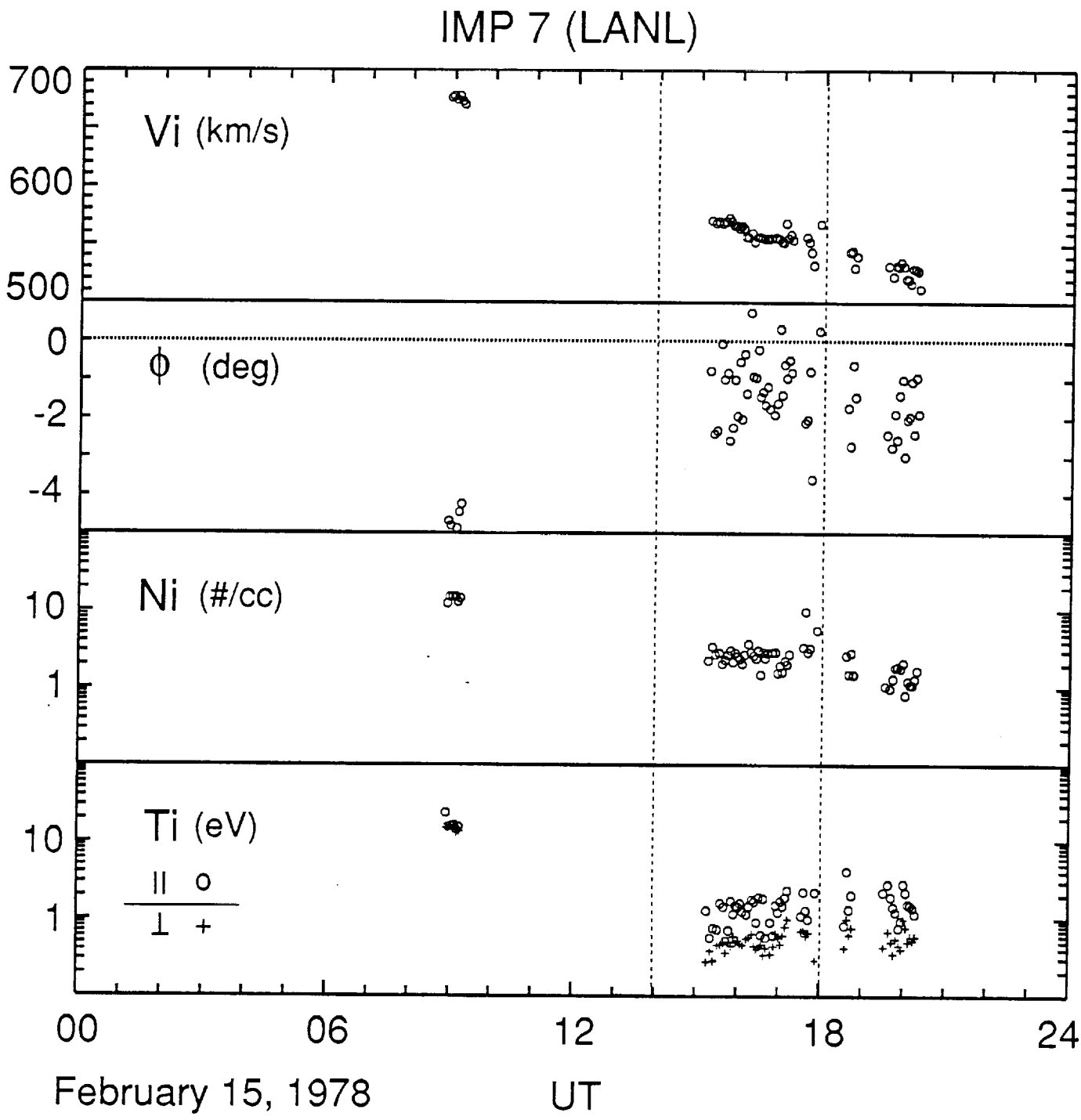
IMP 7 (LANL)
700
600
500
Vi (km/s)
0
-2
-4
ϕ (deg)
10
1
Ni (#/cc)
10
1
Ti (eV)
|| o
⊥ +
00
06
12
18
24
February 15, 1978
UT

Figure 2*a*

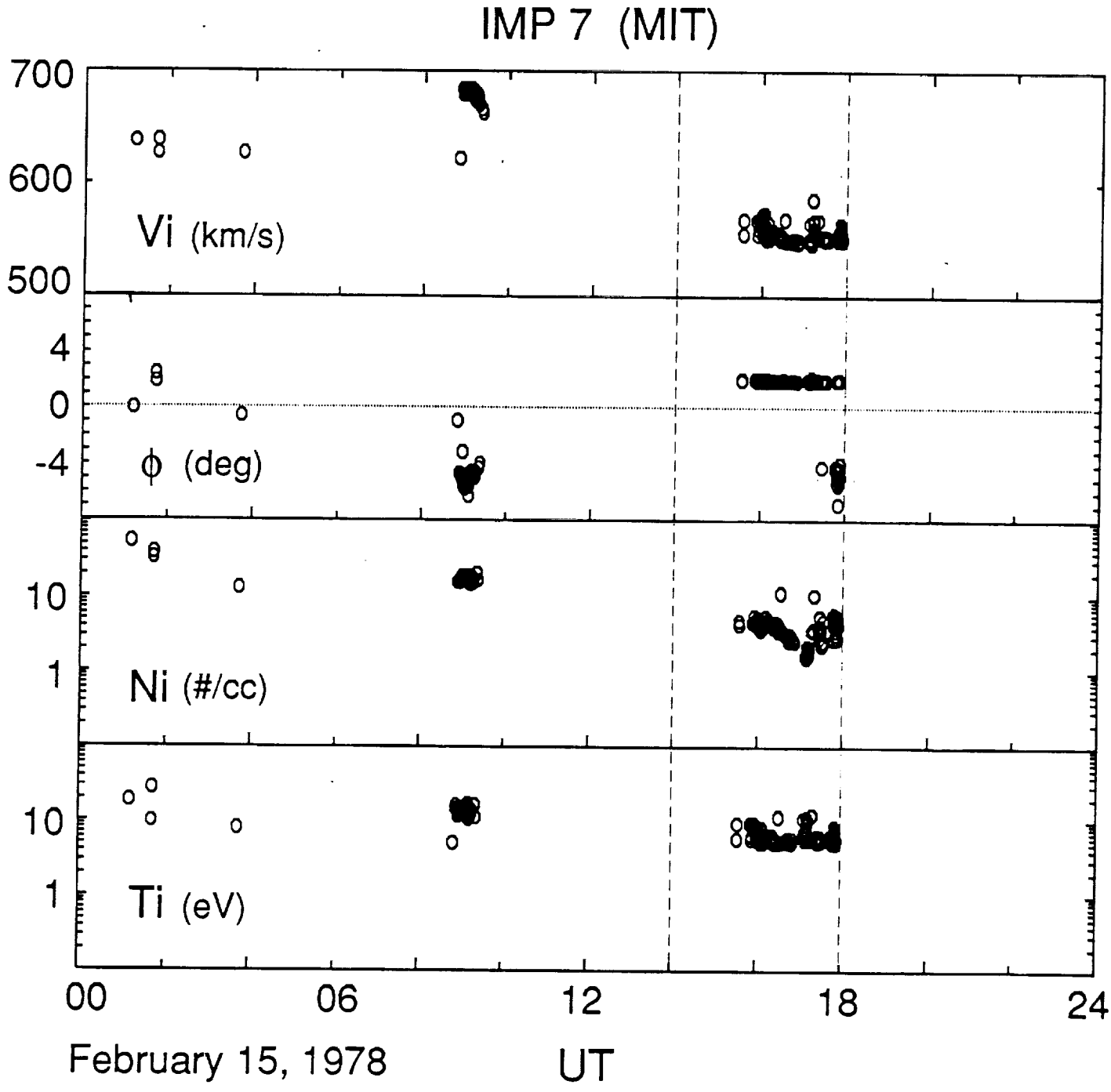
IMP 7 (MIT)
700
600
500
Vi (km/s)
4
0
-4
ϕ (deg)
10
1
Ni (#/cc)
10
1
Ti (eV)
00
06
12
18
24
February 15, 1978
UT

Figure 2*b*

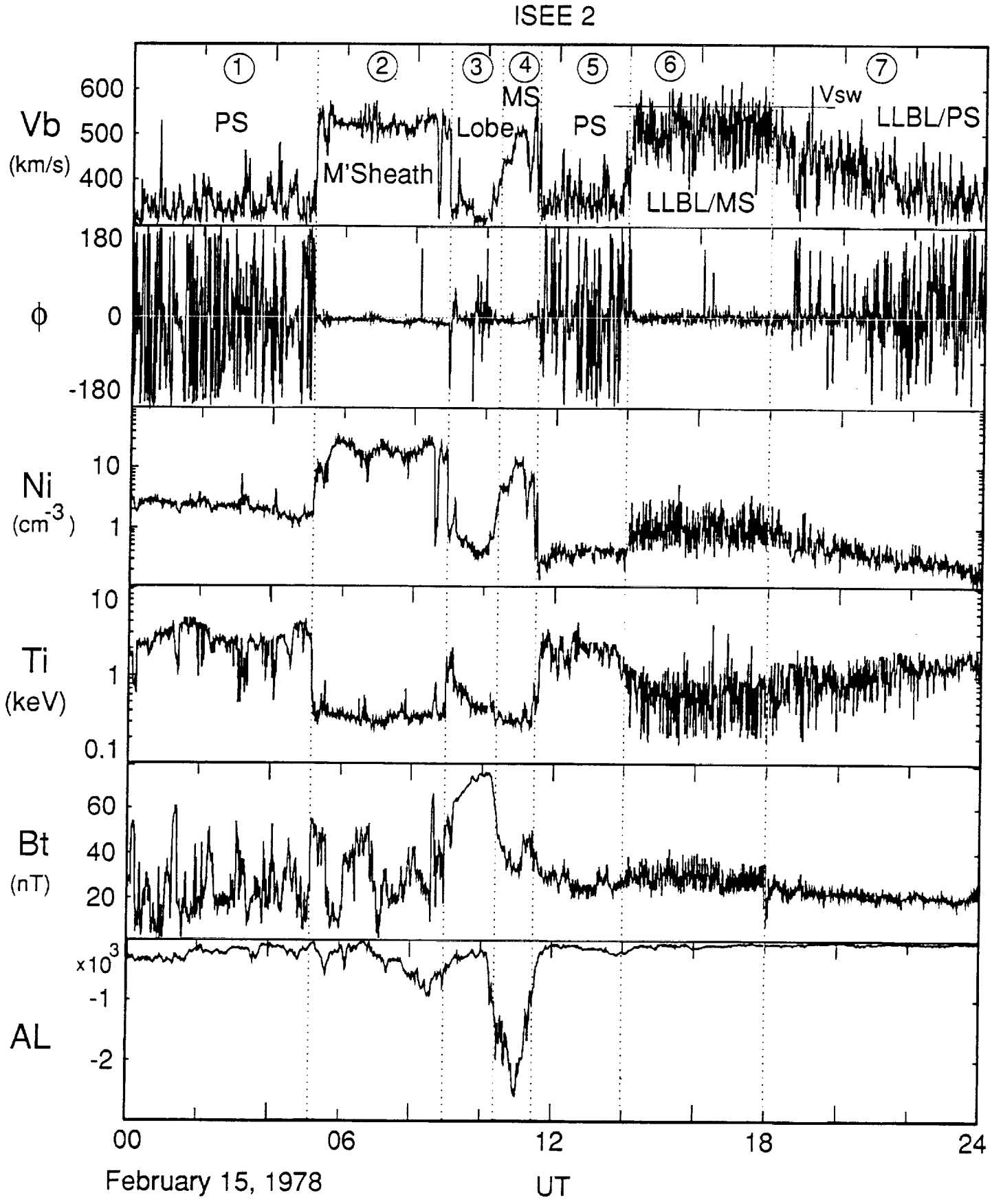
ISEE 2
1
2
3
4
5
6
7
PS
M'Sheath
Lobe
MS
PS
LLBL/MS
Vsw
LLBL/PS
Vb
(km/s)
600
500
400
ϕ
180
0
-180
Ni
(cm-3)
10
1
Ti
(keV)
10
1
0.1
Bt
(nT)
60
40
20
AL
x10^3
-1
-2
00
06
12
18
24
February 15, 1978
UT

Figure 3

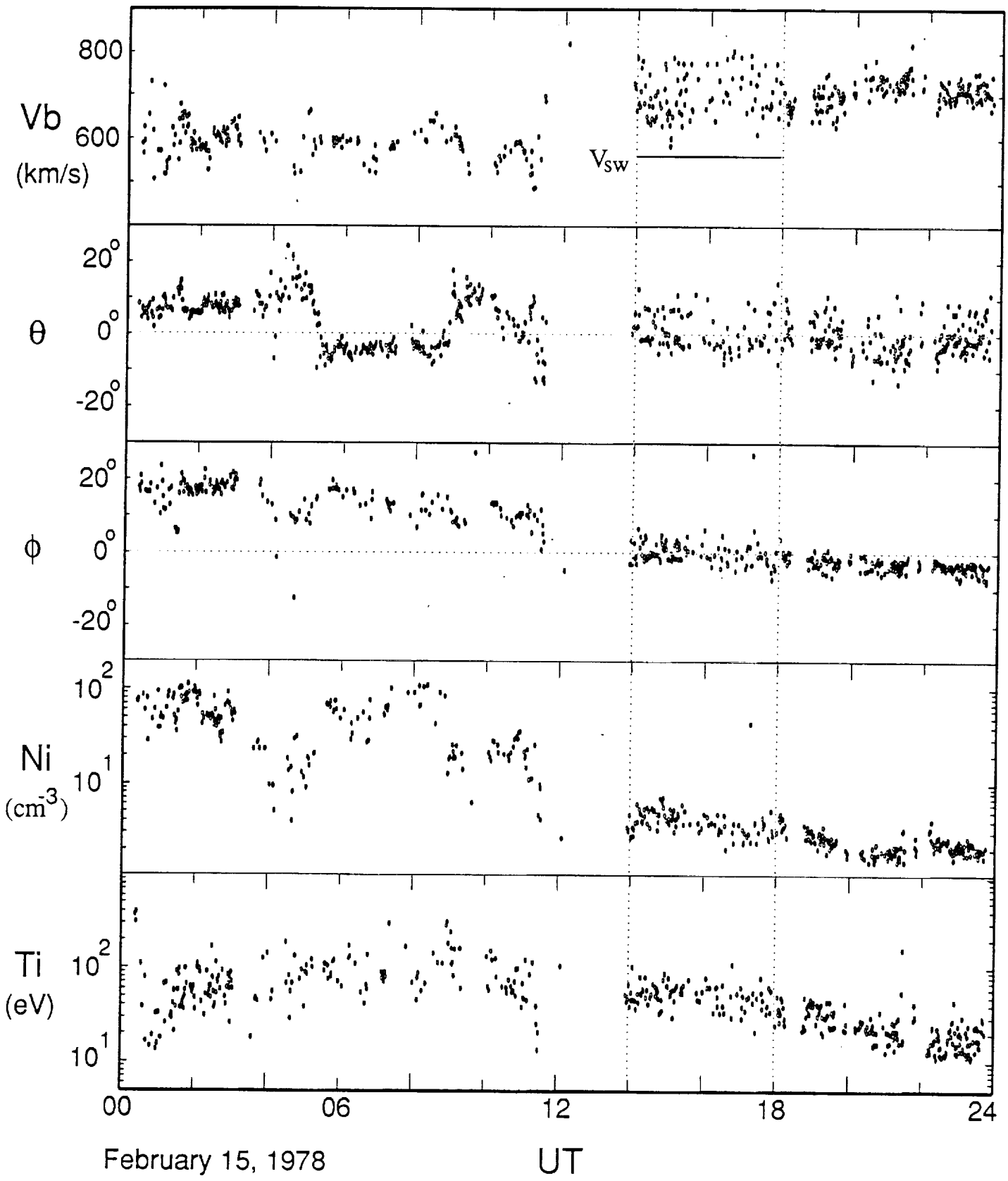
IMP 8 (MIT)
Vb
(km/s)
800
600
V_{sw}
θ
20°
0°
-20°
ϕ
20°
0°
-20°
Ni
(cm^{-3})
10^2
10^1
Ti
(eV)
10^2
10^1
00
06
12
18
24
February 15, 1978
UT
(ϕ : + fr W to E, Aberr. Corrected; θ : fr S to N)

Figure 4

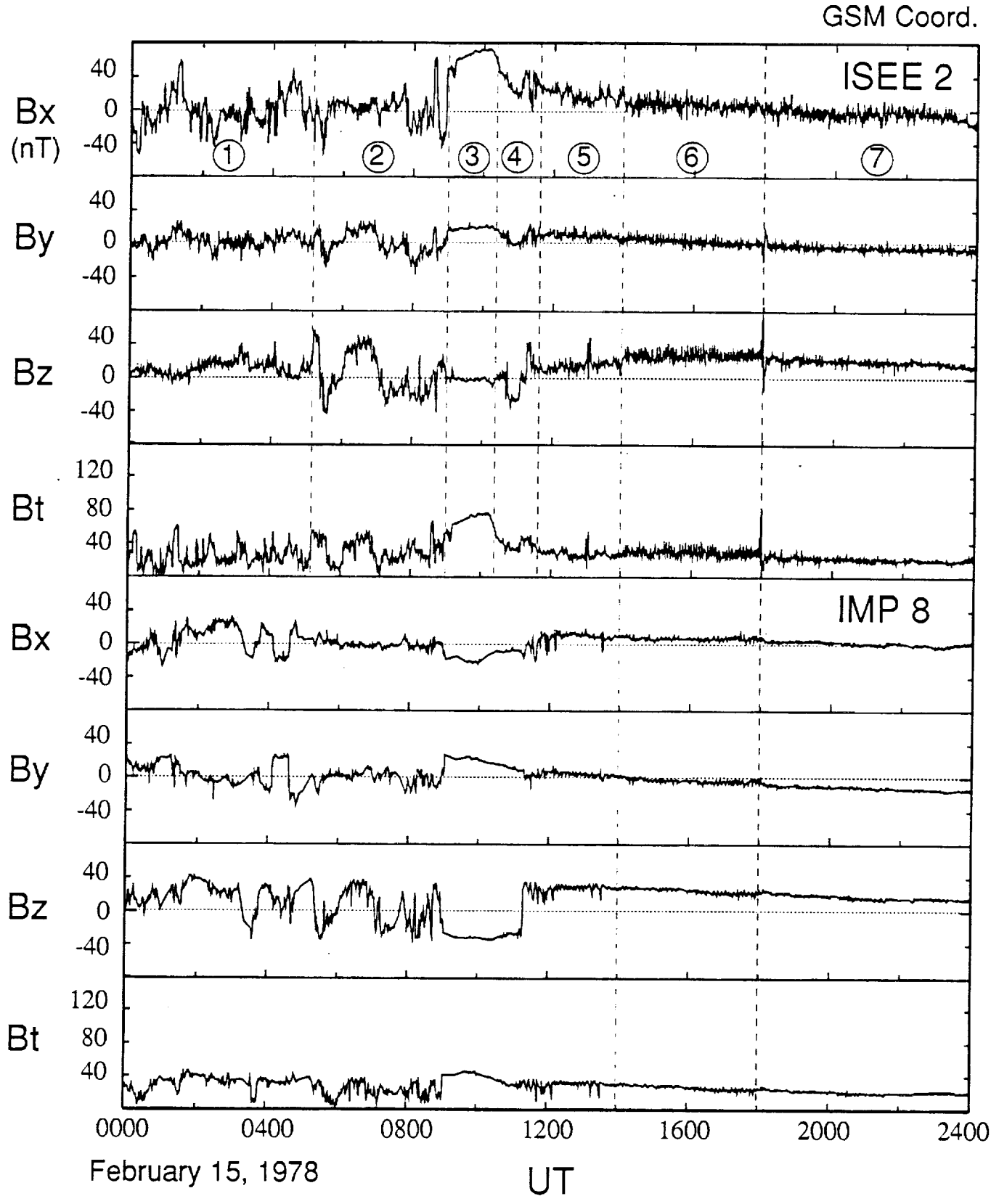
GSM Coord.
ISEE 2
Bx
(nT)
By
Bz
Bt
IMP 8
Bx
By
Bz
Bt
40
0
-40
120
80
40
①
②
③
④
⑤
⑥
⑦
0000
0400
0800
1200
1600
2000
2400
February 15, 1978
UT

Figure 5

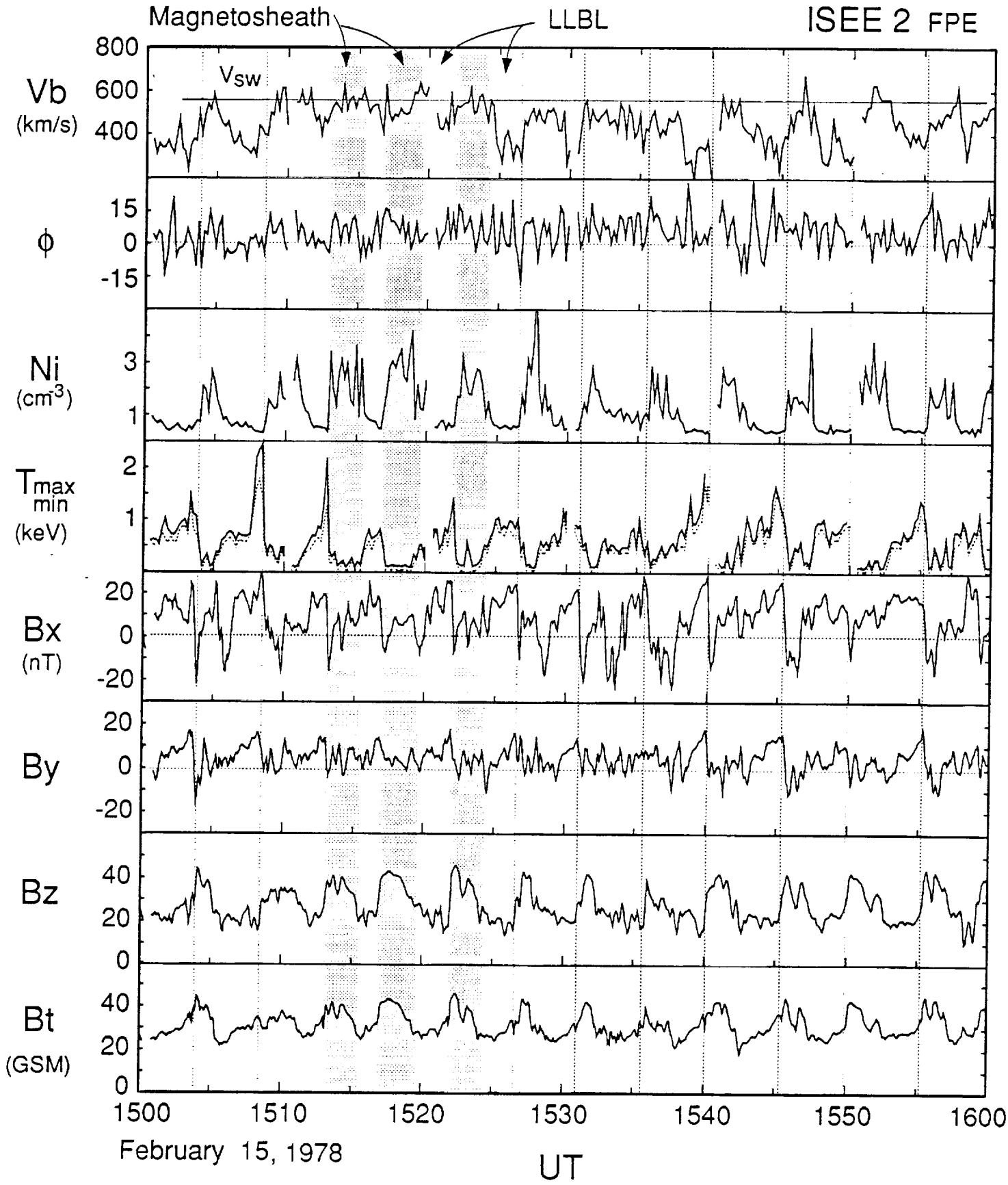
Magnetosheath
LLBL
ISEE 2 FPE
Vb
(km/s)
800
600
400
Vsw
ϕ
15
0
-15
Ni
(cm-3)
3
1
Tmax
min
(keV)
2
1
Bx
(nT)
20
0
-20
By
20
0
-20
Bz
40
20
0
Bt
(GSM)
40
20
0
1500
1510
1520
1530
1540
1550
1600
February 15, 1978
UT

Figure 6

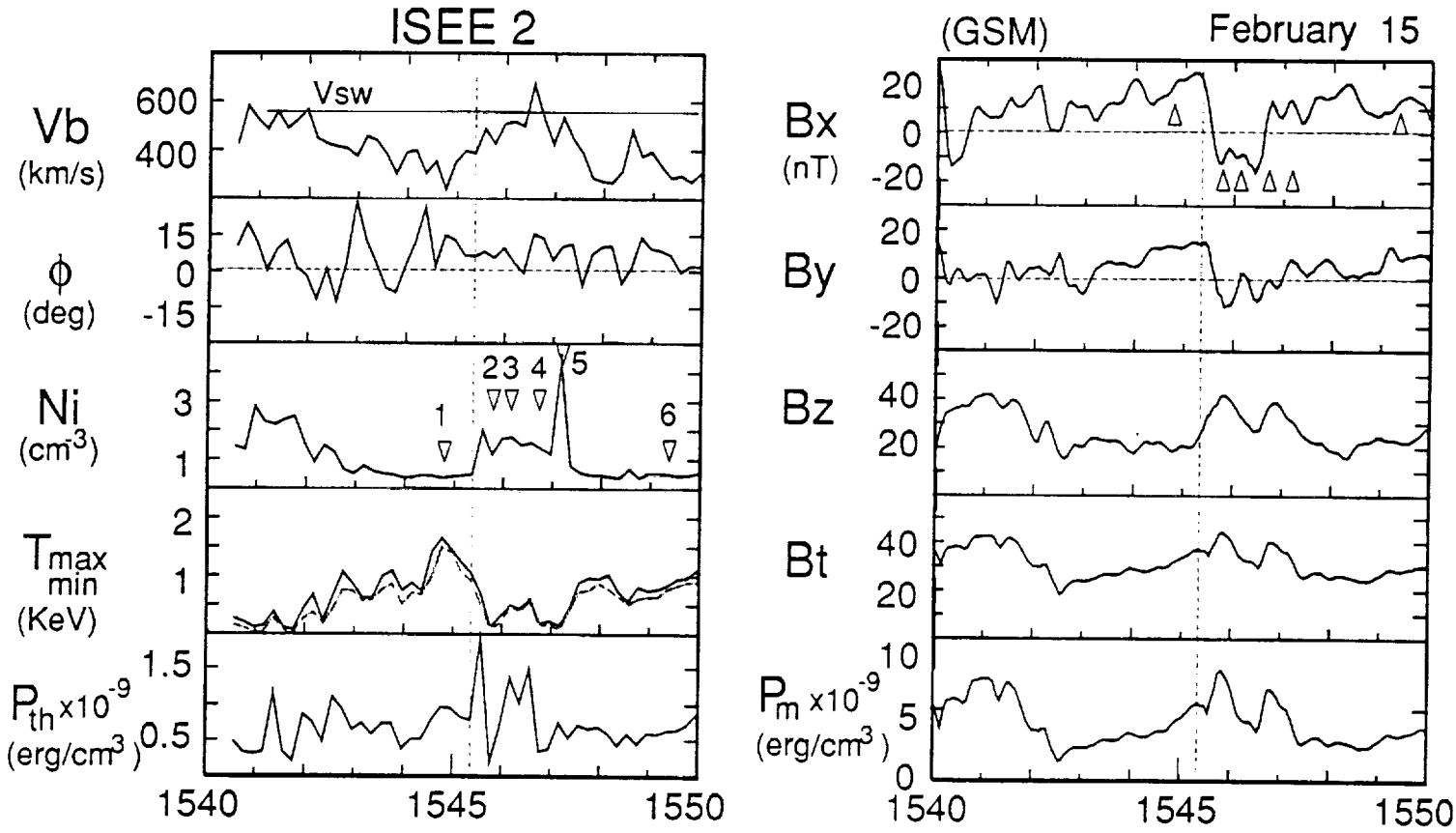
ISEE 2
(GSM)
February 15
Vb
(km/s)
600
400
Vsw
ϕ
(deg)
15
0
-15
Ni
(cm^3)
3
1
1
2 3 4
5
6
Tmax
min
(KeV)
2
1
Pth x10^{-9}
(erg/cm^3)
1.5
0.5
Bx
(nT)
20
0
-20
By
20
0
-20
Bz
40
20
Bt
40
20
Pm x10^{-9}
(erg/cm^3)
10
5
0
1540
1545
1550

Figure 7*a*

780215 15:44:45–48

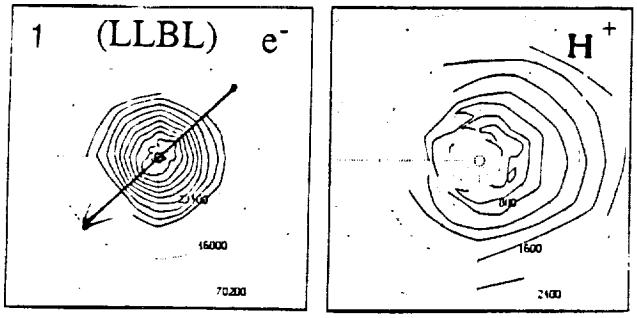

780215 15:45:45–48

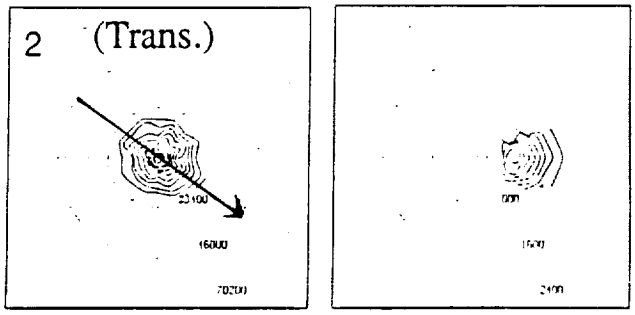

780215 15:46:09–12

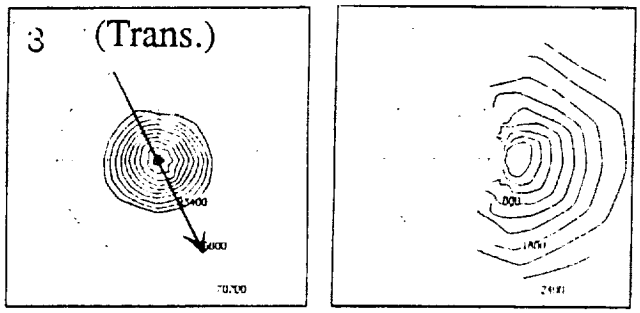

780215 15:46:45–48

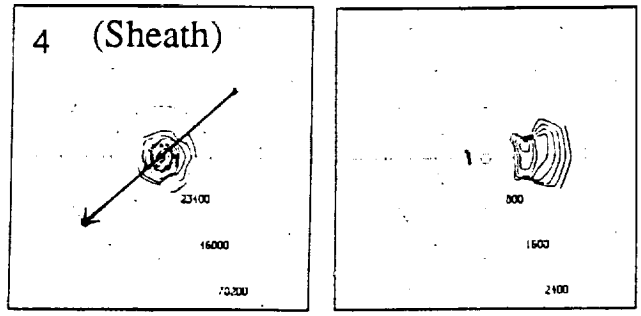

780215 15:47:09–12

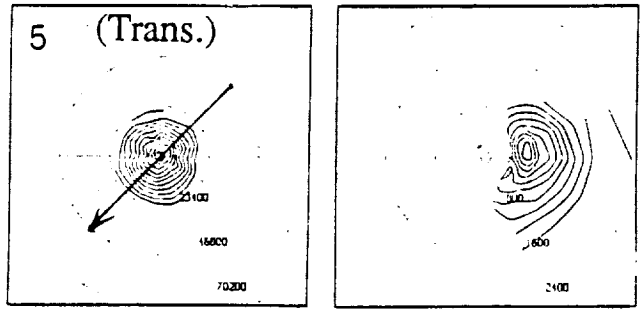

780215 15:49:21–24

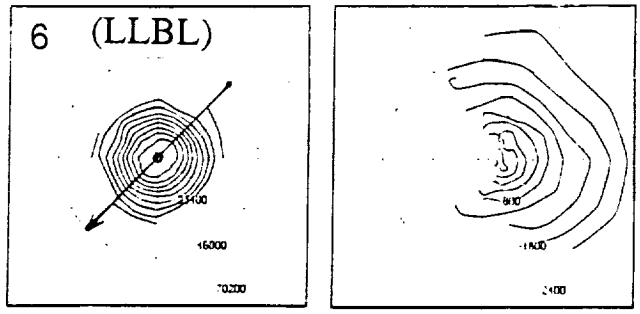

Figure 7*b*

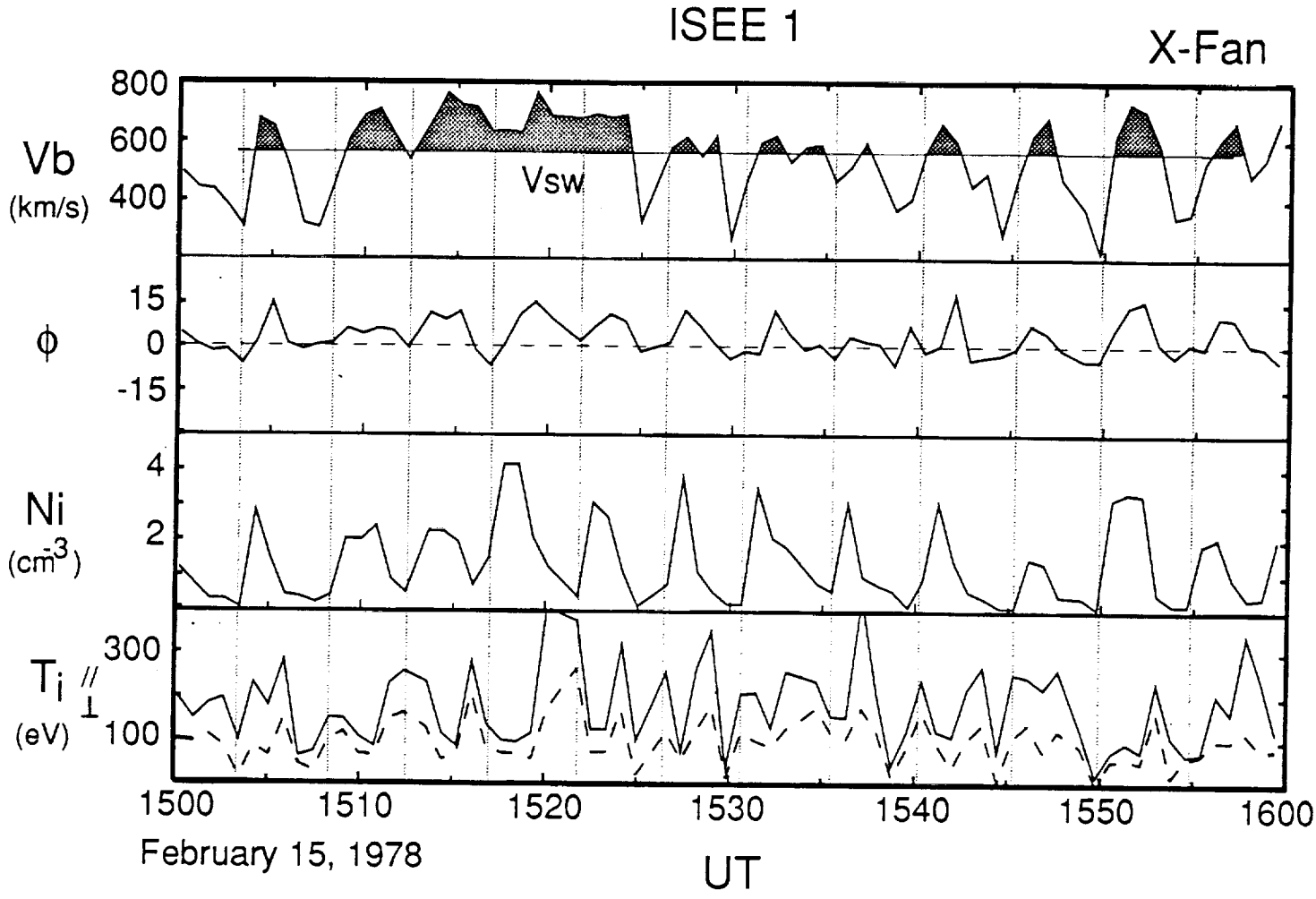
ISEE 1
X-Fan
Vb
(km/s)
800
600
400
Vsw
ϕ
15
0
-15
Ni
(cm-3)
4
2
Ti //
⊥
(eV)
300
100
1500
1510
1520
1530
1540
1550
1600
February 15, 1978
UT

Figure 8

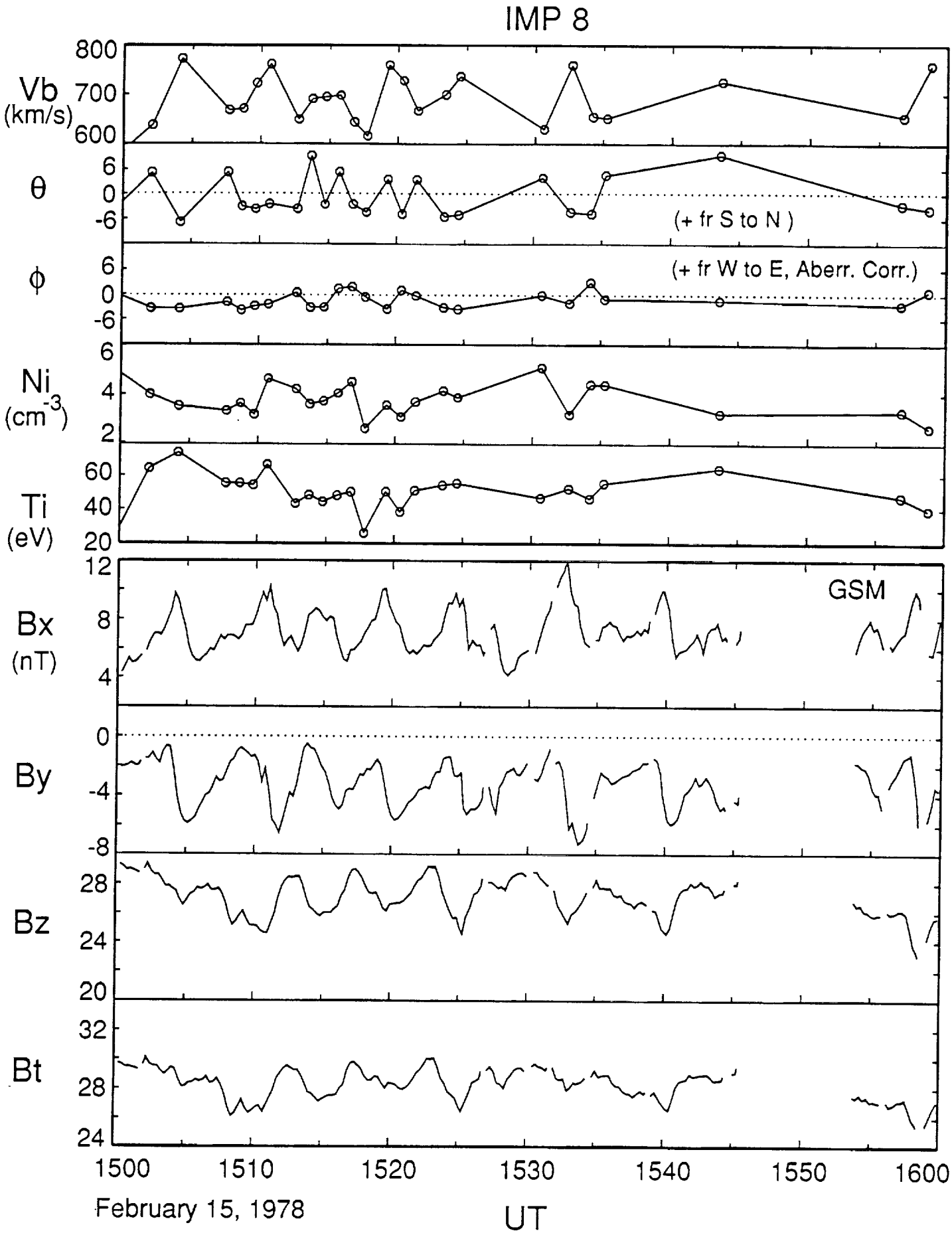
IMP 8
Vb
(km/s)
800
700
600
θ
6
0
-6
(+ fr S to N)
ϕ
(+ fr W to E, Aberr. Corr.)
Ni
(cm-3)
Ti
(eV)
60
40
20
GSM
Bx
(nT)
12
8
4
By
-4
-8
Bz
28
24
20
Bt
32
28
24
1500
1510
1520
1530
1540
1550
1600
February 15, 1978
UT

Figure 9

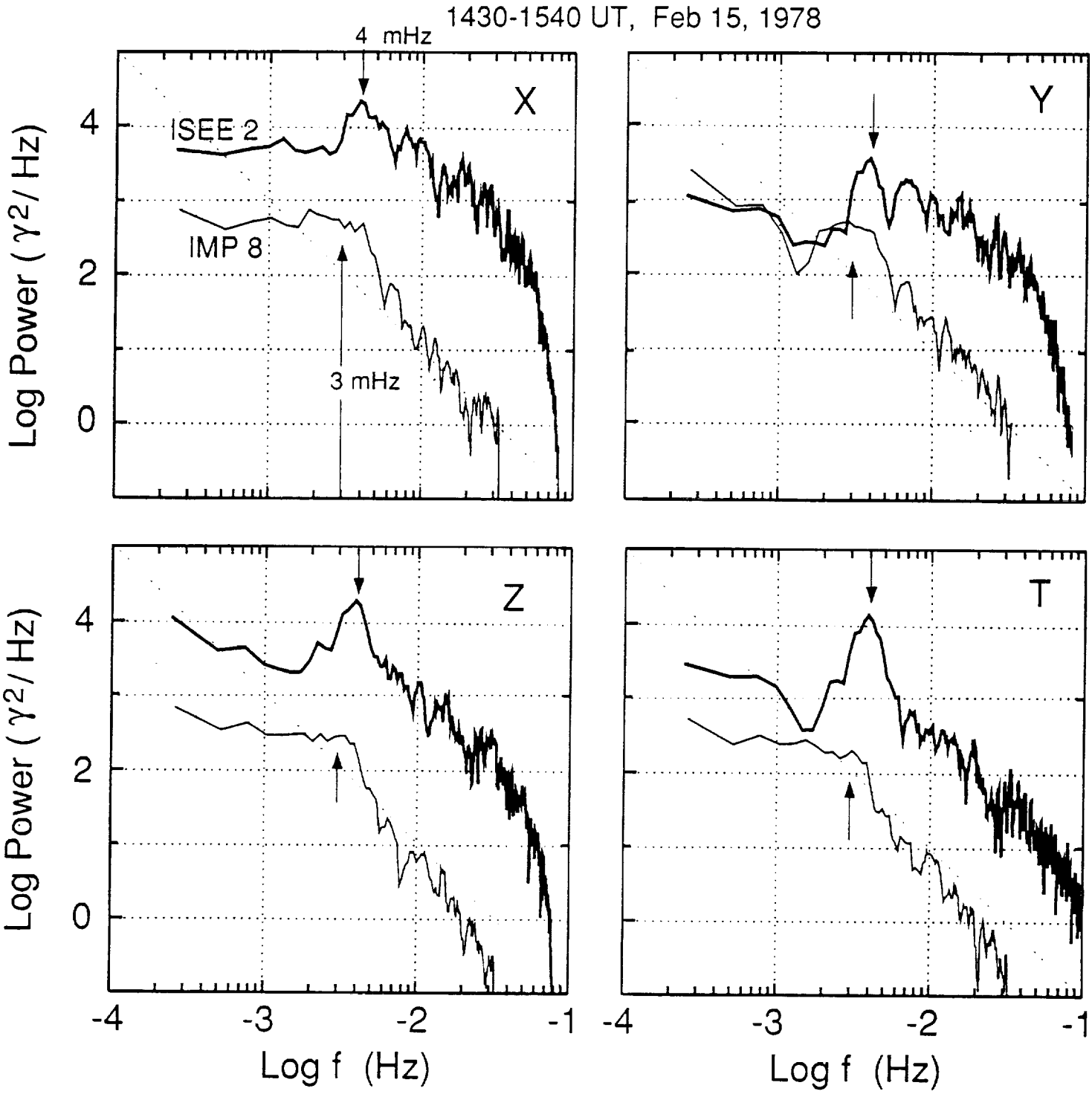
1430-1540 UT, Feb 15, 1978
4 mHz
X
Y
Z
T
ISEE 2
IMP 8
3 mHz
Log Power (γ2/ Hz)
Log f (Hz)
4
2
0
-4
-3
-2
-1

Figure 10

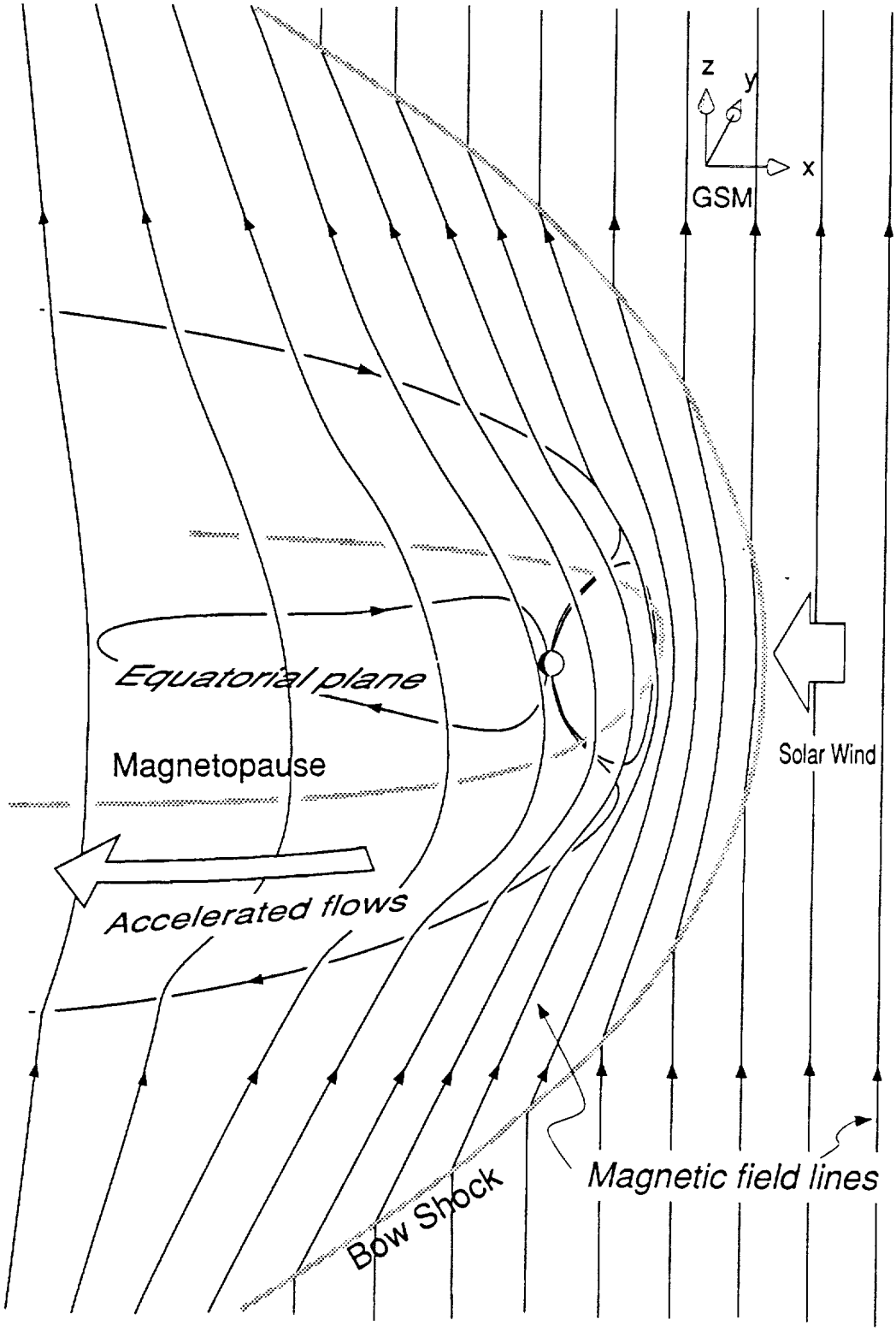
z
y
x
GSM
Equatorial plane
Magnetopause
Solar Wind
Accelerated flows
Bow Shock
Magnetic field lines

Figure 11

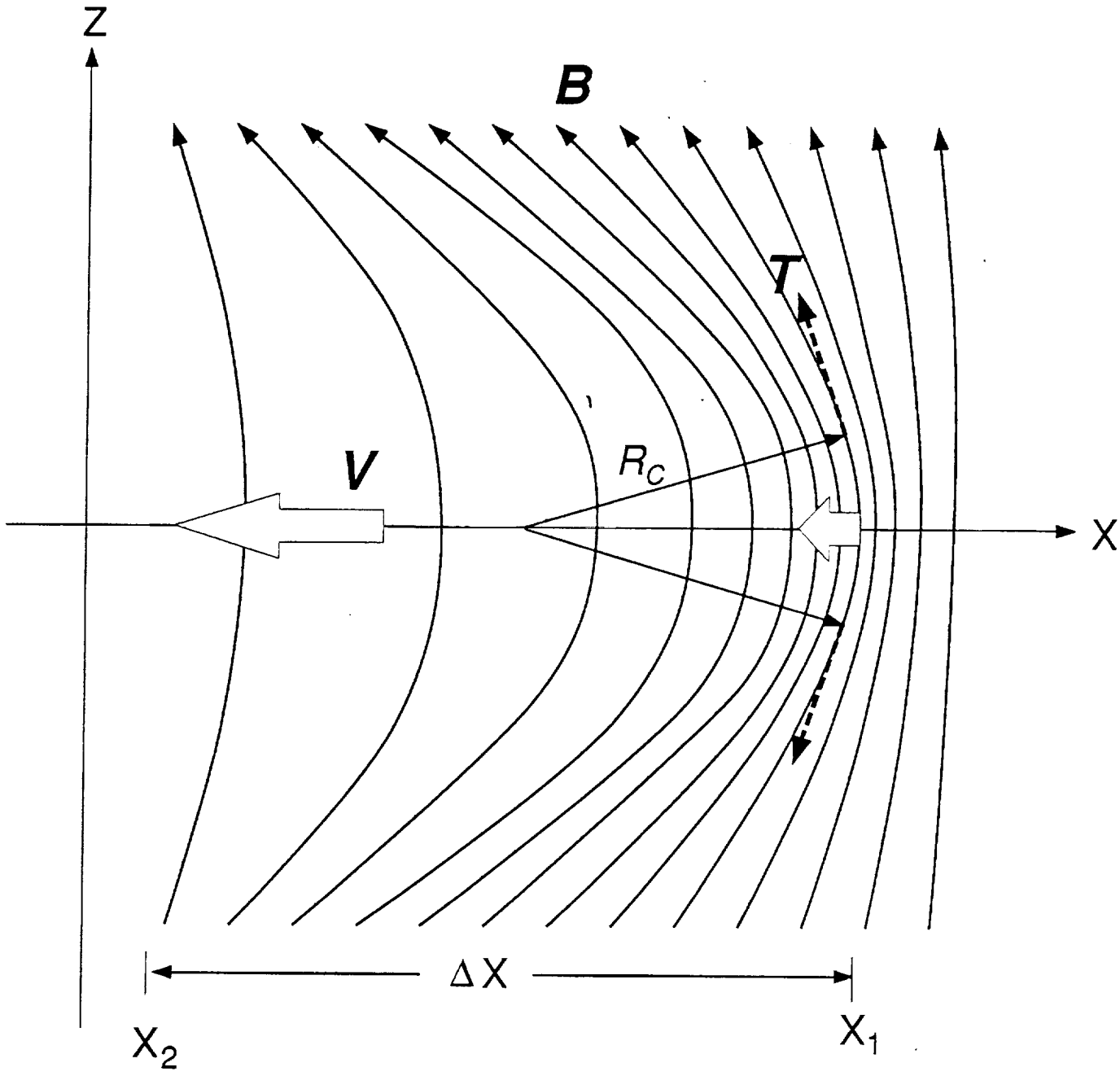

Figure 12

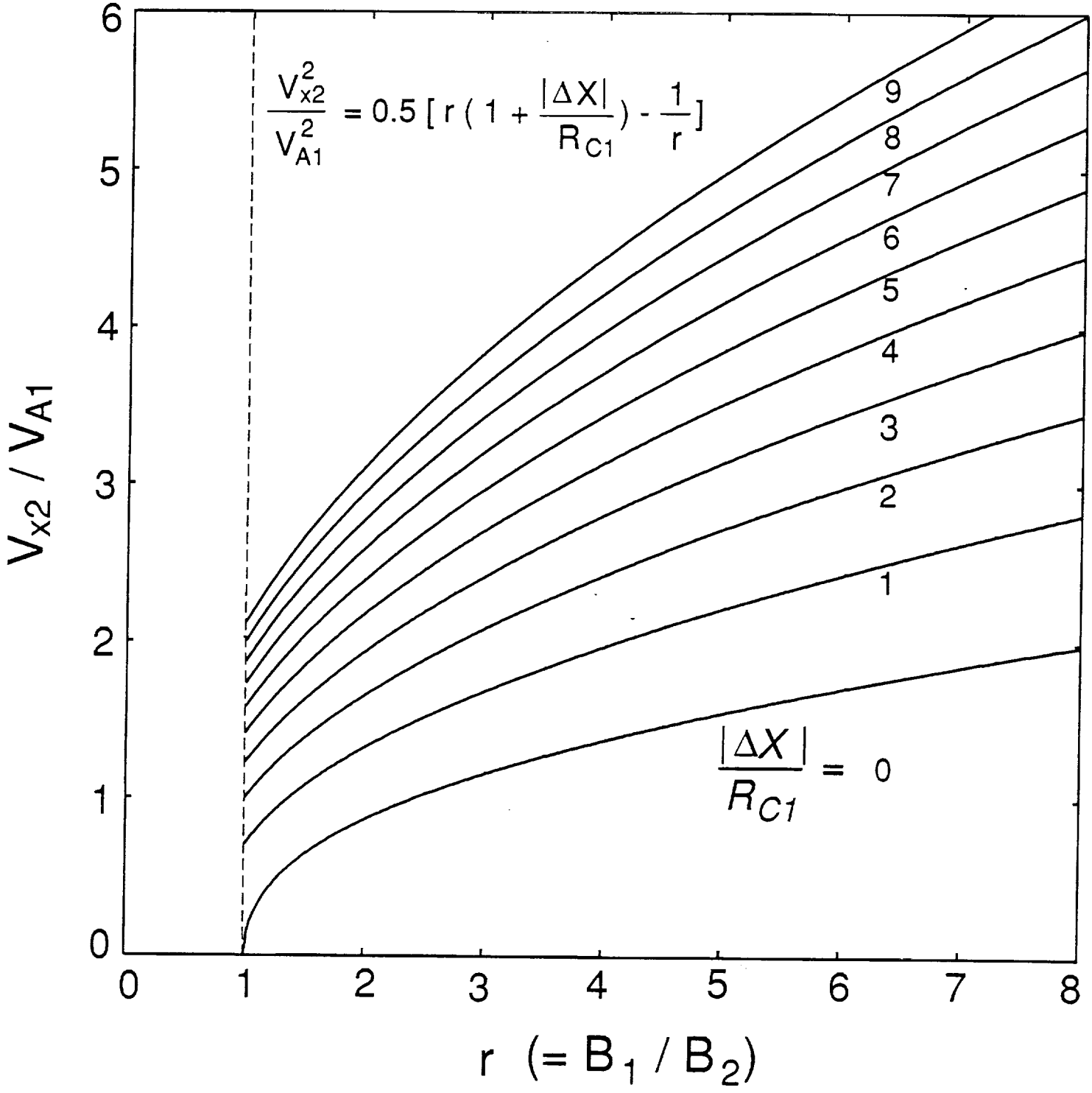
$\frac{V_{x2}^2}{V_{A1}^2} = 0.5\,[\,r\,(\,1 + \frac{|\Delta X|}{R_{C1}}) - \frac{1}{r}\,]$
9
8
7
6
5
4
3
2
1
$\frac{|\Delta X|}{R_{C1}} = 0$
V_{x2} / V_{A1}
$r\ (= B_1 / B_2)$
0
1
2
3
4
5
6
7
8

Figure 13

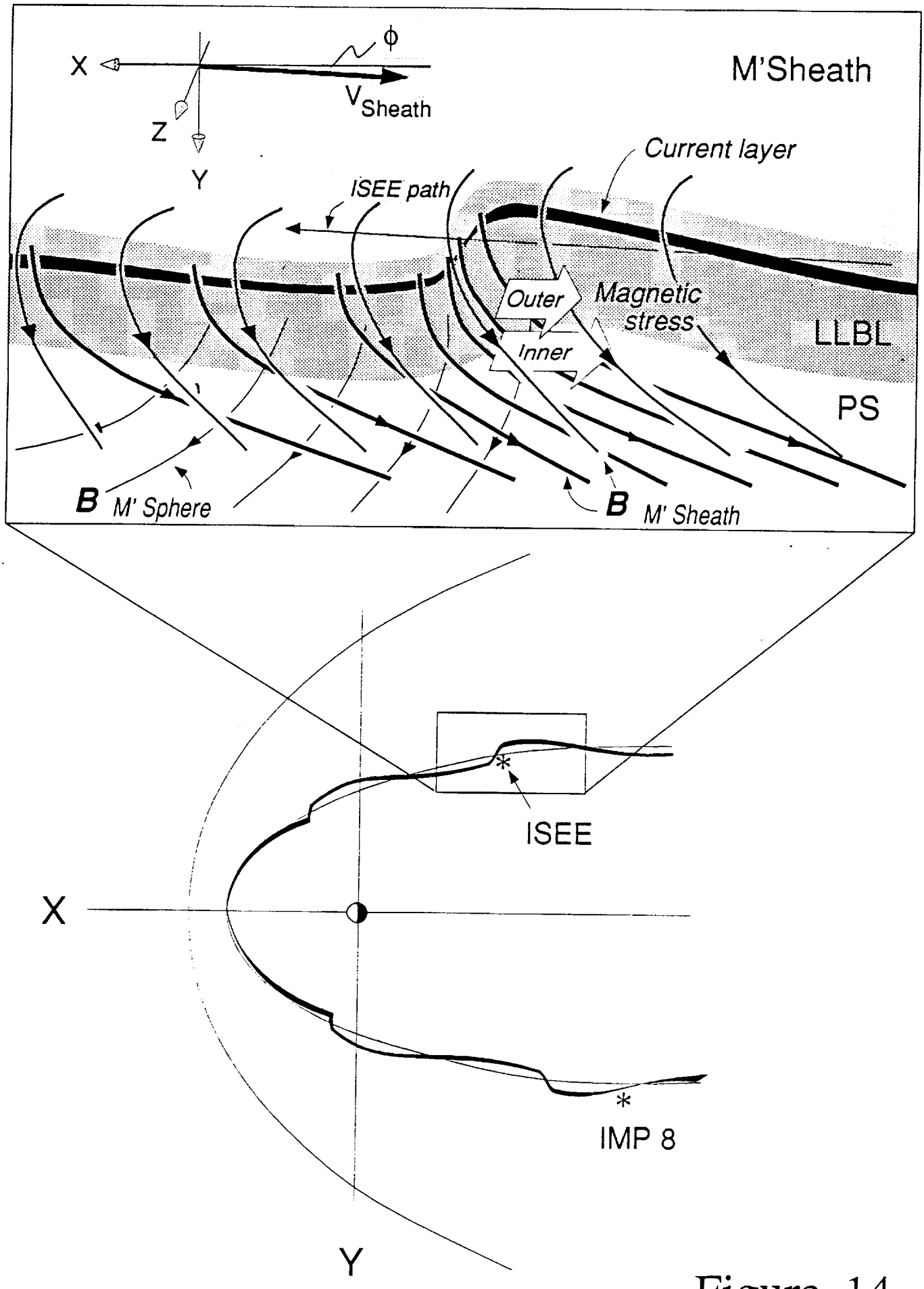
X
ϕ
V Sheath
Z
Y
M'Sheath
Current layer
ISEE path
Outer
Inner
Magnetic stress
LLBL
PS
B M' Sphere
B M' Sheath
ISEE
X
IMP 8
Y

Figure 14

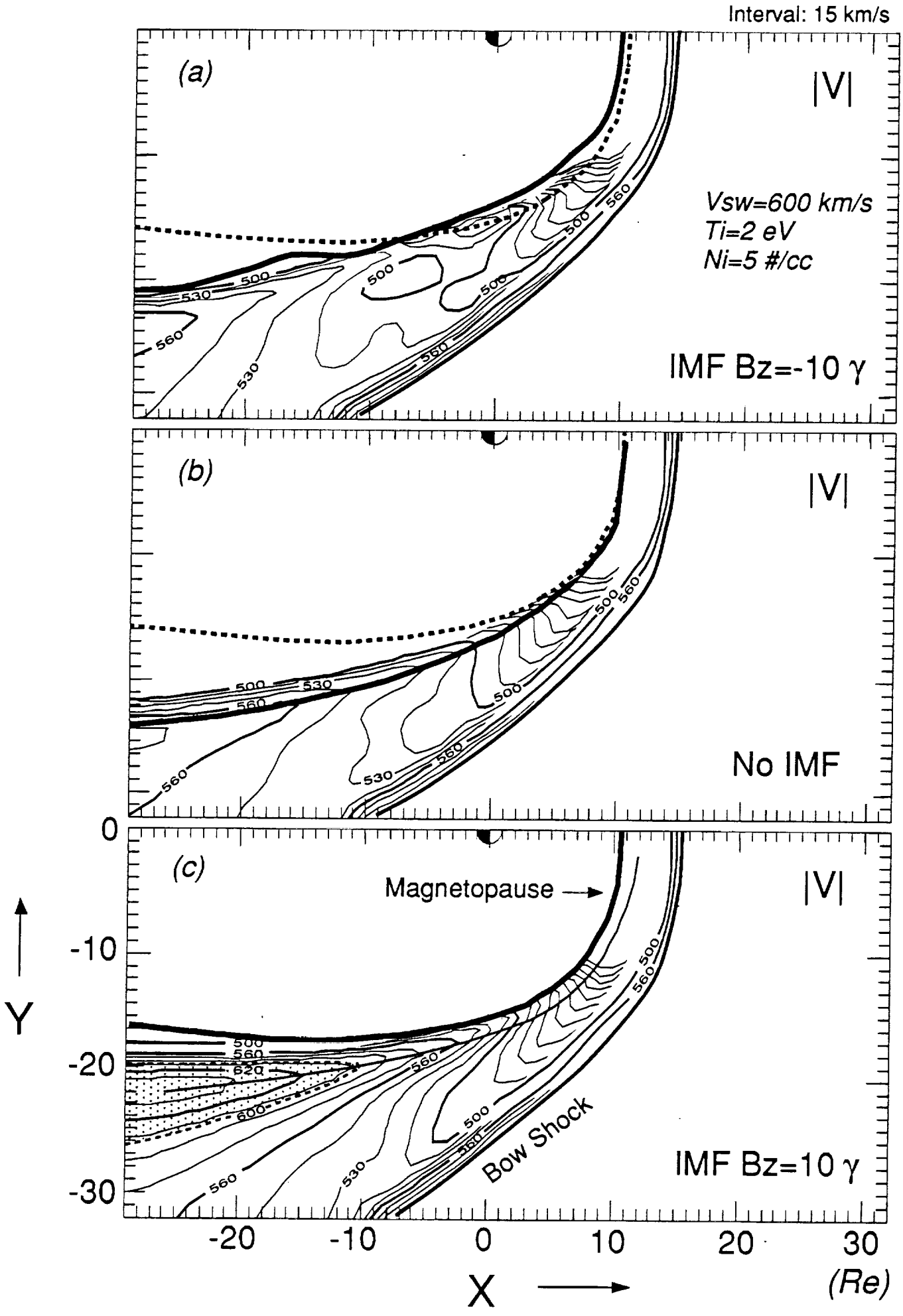
Interval: 15 km/s
(a)
|V|
Vsw=600 km/s
Ti=2 eV
Ni=5 #/cc
IMF Bz=-10 γ
(b)
|V|
No IMF
(c)
|V|
Magnetopause
Bow Shock
IMF Bz=10 γ
0
-10
-20
-30
Y
-20
-10
0
10
20
30
X
(Re)

Figure 15

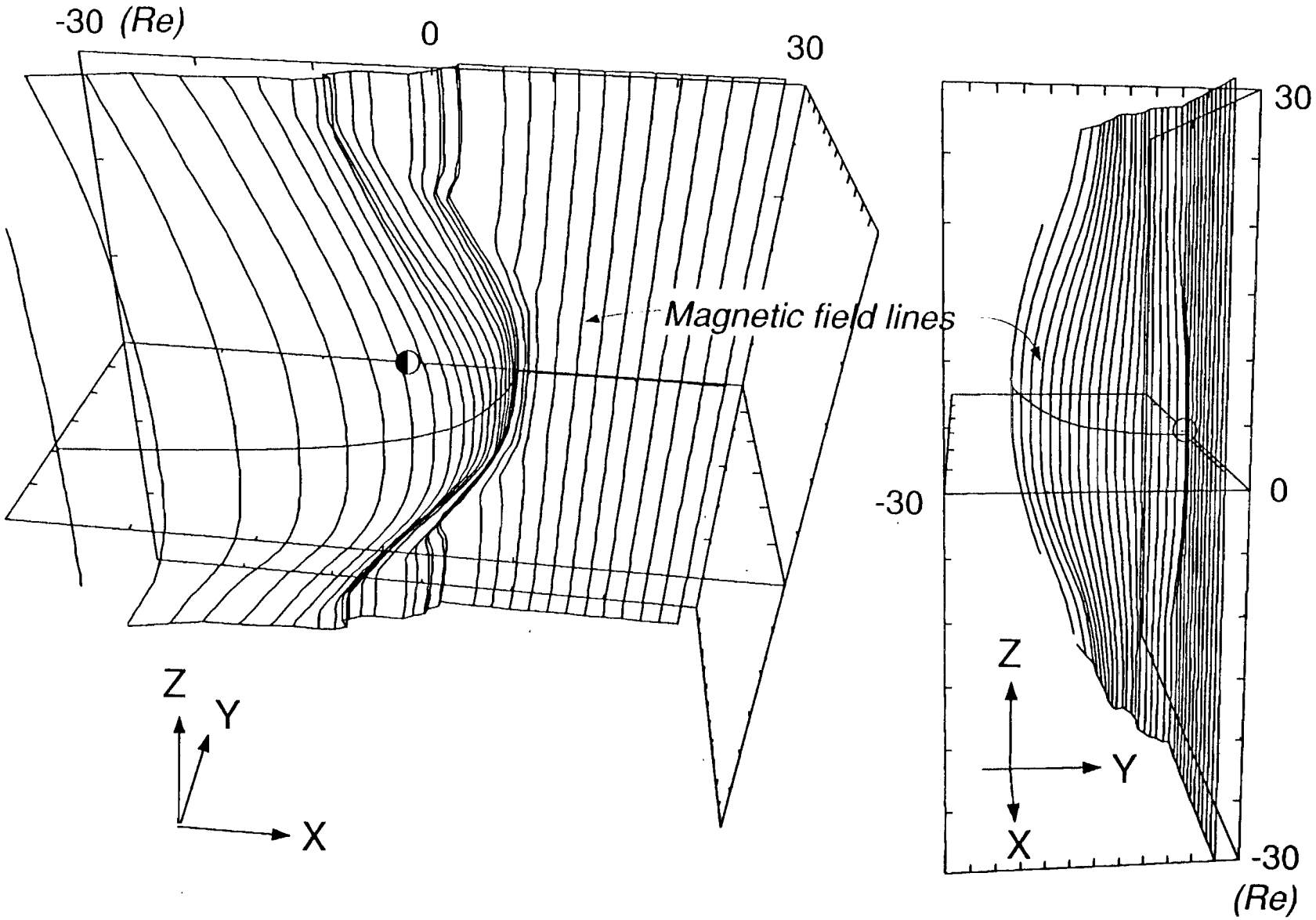

Figure 16